Impacts of Torrefaction and Ash Reduction on the Catalytic Fast Pyrolysis of Energy Crops

by

Thomas Brett Beery

(Under the Direction of Sudhagar Mani)

Abstract

Energy crops containing a large fraction of alkaline metals produce low-quality bio-oil during pyrolysis. In this study, effects of alkali metal reduction on catalytic fast pyrolysis of Napier grass were investigated. Also, a thermal pretreatment, torrefaction, was investigated for its effect on reducing coke formation and oxygen content of pyrolysis oil produced from demineralized feedstock. An in-situ catalytic fast pyrolysis process was developed using red mud, a waste material from aluminum production, as a catalyst. A simple water washing method reduced total ash content and alkaline metals content by more than 50% (wt). Reduction of alkaline metal in biomass increased levoglucosan concentration up to 200+ g/L in bio-oil without a catalyst. Alternatively, overall concentrations of levoglucosan, acetate, and formate were reduced with torrefaction pretreatment and catalytic pyrolysis. Further research is required to optimize the yields of water soluble fractions in bio-oil with reduced alkaline metals in the energy crops.

Index words: Catalytic Pyrolysis, Red Mud, Torrefaction, Water Washing, Napier Grass

Impacts of Torrefaction and Ash Reduction on the Catalytic Fast Pyrolysis of Energy Crops

by

Thomas Brett Beery

B.S in Biochemistry and Molecular Biology, University of Georgia, 2010

A Thesis Submitted to the Graduate Faculty of The University of Georgia in Partial Fulfillment of the Requirements for the Degree

MASTER OF SCIENCE

ATHENS, GEORGIA

2016

Impacts of Torrefaction and Ash Reduction on the Catalytic Fast Pyrolysis of Energy Crops

by

Thomas Brett Beery

Major Professor:	Sudhagar Mani
Committee:	James Kastner
	K.C. Das

Electronic Version Approved:

Suzanne Barbour
Dean of the Graduate School
The University of Georgia
December 2016

Dedication

Dedicated to my Grandparents, Tom and Juanita Beery, and my mother, Elsie Beery, who have always pushed me to strive towards higher goals and supported me throughout my years.

Acknowledgments

I would like to think my fellow graduate students for their support, both on good days and bad. Thank you to Joby Miller, for doing all she could, and then some, with helping me on the GC-MS and giving me a deeper understanding of it. Thank you to Sarah Lee for all her extensive help with using the HPLC in Dr. Eiteman's lab. I am extremely grateful to Terry Walsh, the research machinist, who put up with my myriad of questions and requests to throw scrap metal together and make wonders.

I especially want to thank Dr. Roger Hilten for all of the support and confidence he has shown me throughout the project. Many months of time were saved, and even more, vast knowledge was gained through our many conversations. I leave this work behind with a deeper level of insight, and a stronger understanding of good, quality research thanks to his kindness.

This project was financially supported by the USDA-NIFA sustainable bioenergy research grant number GEOX-2010-03868 via Fort Valley State University.

Contents

List of Tables

List of Figures

Chapter 1

Introduction

Biomass an alternative source of renewable fuels to replace fossil fuels due to its potential to reduce greenhouse gas (GHG) emissions and enhance local economic development. Also, biomass has negligible amounts of sulfur and nitrogen, which leads to reduced emissions of SO_2 and NO_x. Further, biomass is considered carbon-neutral, because CO_2 emitted from combustion is prepaid by plant absorption during photosynthesis. The U.S. Department of Energy's Billion-Ton Update estimates 255 million dry tons of perennial grasses to be produced in 2030 at \$60/dry ton from non-food crop-lands or marginal lands [1]. This is approximately twice as much dry mass as is predicted to be available from woody crops. With such production of crops for energy, the issue of low-quality conversion must be addressed.

Energy crops are non-woody plants that are specifically bred for use in the production of energy. They are not food crops and can be grown on non-agricultural lands. Thus, they provide a plant-based fuel source, without competing with food production. Within this classification of plants, there are traits which are desirable to increase the production yield and lower costs, e.g. tillage requirements and fertilizer application [2, 3]. Perennial plants are favored over annuals for their low tillage need and the addition of carbon to the soil. Perennial root systems, additionally, help to mitigate soil erosion. For this reason, C4

plants are considered superior to C3 plants. Common C4 crops include sugarcane, energy cane, Elephant or Napier grass, switchgrass, and Miscanthus. Energy crops are bred from these plants, crossing various strains to generate a progeny with beneficial traits. These traits vary by location. Typical ones include reduced water and fertilizer requirements, increased lignocellulosic mass production, cold tolerance, disease resistance, and extending harvest times. While it is unlikely that one single crop will become the universal supplier of all bioenergy, this research will focus primarily on elephant grass [4–8]. *Pennisetum Purpureum*, also called Napier grass or elephant grass, is a C4 perennial grass native to Africa. It has low supplemental nutrient requirements and has growth rates reported to be 30-40 dry tons/ha/yr and can be harvested multiple times per year [9–11].

1.1 Rationale

Biomass has low bulk density, high moisture content, and low energy density when compared to coal [12, 13]. These three elements create problems for transport, storage, and conversion. Much research has been devoted to alleviating these problems from a wide angle of possibilities. Thermochemical conversions,specifically pyrolysis technologies, are already used in the petroleum industry, and it is desirable to create a product that can take advantage of these infrastructures. These treatments use heat, typically under inert conditions to prevent combustion, to break down biomass into more desirable products. This conversion pathway is not without its own drawbacks, as liquid products from thermal processes suffer from high moisture and oxygen content, low pH, and low HHV [14–17].

This study will look into thermochemical conversions in the form of fast pyrolysis via a fluidized bed reactor, and torrefaction via a batch process using a furnace. Fast pyrolysis is a thermochemical conversion process whereby mass is heated, typically 400-600°C, in the absence of oxygen with a short residence time, on the order of seconds. The torrefaction

process uses a lower temperature, between 200-300°C, and longer hold times of several minutes under inert conditions. Fast pyrolysis, followed by hydroprocessing, is utilized in the NREL [18] Techno-economic assessment of biomass to produce transportation fuel and electricity. This processing scheme [19] was found to be capable of producing the cheapest gallon of gasoline equivalent (GGe) out of three studies done at Iowa State University [19–21]. The NREL study provides a model whereby gasoline could be produced for $2.57/gal. A sensitivity analysis showed that both bio-oil yield and fuel yield had the highest impact on the selling price [18]. As such, advancements that increase yields and yield quality, e.g. improved stability or HHV, would provide a lower cost fuel assuming that the improvement itself was not of equal or greater cost. This research will investigate the use of torrefaction as a pretreatment to fast pyrolysis, used in tandem with an in-situ catalyst to further enhance oil quality.

As previously mentioned, pyrolysis oils suffer from high moisture content, high oxygen content, low pH, and low HHV that label it as lower quality than fossil fuel counterparts without further upgrading. One of the issues with bio-oil is its pH value, which for bio-oil are typically reported to be 2-4 [22–24]. This creates problems with storage and transport due to corrosion of pipes and containers (e.g. corrosion of carbon steel). This problem must be corrected to provide high-quality fuels that are capable of replacing gasoline. Additionally, pyrolysis oils have higher moisture content, typically 15-30%, and oxygen content, typically 35-40%, than fossil fuel counterparts, resulting in a decreased HHV, as well as issues with degradation in long-term storage [15–17].

This research aims to mitigate these issues, by pretreating biomass with torrefaction, and by using a catalyst in-situ to generate a higher quality oil from fast pyrolysis. The analytical chemistry techniques described herein will be used to determine significant changes to the oxygen and pH content of the bio-oil produced. This differs from conventional methods which generate a lower quality oil that requires heavy upgrading downstream. Torrefaction causes

the evolution of biomass constituents, in particular degrading hemicelluloses and cellulose depending on the temperature. Reduction of these groups could help to screen out some of the organic acids produced from fast pyrolysis, aiding in pH and oxygen content levels. However, with this reduction comes an overall mass deficit, as well as increased energy input, which must be considered when evaluating the end product of fast pyrolysis.

It is desired to attempt and further reduce the oxygen content of the pyrolysis oil product by introducing a catalyst. While research has been conducted in an attempt to find a catalyst to fix various properties of bio-oil, many of the studies have used expensive laboratory catalysts that would be economically prohibitive when used as an in-situ catalyst due to mass requirements. For bio-oil and its subsequent bio-fuel to be competitive with conventional fossil derived transportation fuels, it is necessary to find the cheapest catalyst possible that remains effective. To be economically competitive, the catalyst needs to be inexpensive and resistant to deactivation, or available in such large quantities as to be expendable. Based on this and previous works, red mud is chosen to fill this role.

This study will investigate the use of red mud as a catalyst to decrease the oxygen content of the pyrolysis oil produced. Red mud is an industrial waste from bauxite refining by the Bayer process during the refinement of aluminum. It consists of varying amounts of metal oxides such as Fe_2O_3, Al_2O_3, and SiO_2, among others [25]. The Fe_2O_3 is the major component for red mud and is responsible for the red coloration. Red mud suffers from the opposite problem with bio-oil presented earlier; its pH is very high, 10 to 12 [26]. Because it is not economical to refine, and highly alkaline, it is considered a hazardous waste to the environment. For these reasons, red mud is not expected to carry much if any cost for use as a catalyst in the catalytic fast pyrolysis system. Red mud, as a catalyst, has been studied for a wide variety of purposes. Its array of metal oxides may provide additional cracking benefits unique to catalytic pyrolysis thanks to the presence of Fe_2O_3 and TiO_2 [27]. Other studies have found red mud to be able to catalyze both deoxygenation and cracking reactions

when in a reduced form [28]. Red mud has also been shown to catalytically reduce oxygen and acid content of oils produced while increasing the aromatic content over non-catalytic fast pyrolysis [29].

There are few studies which investigate torrefaction as a pretreatment to fast pyrolysis, of which those are primarily directed at forestry products [30, 31]. Few studies have used torrefaction as a pretreatment to catalytic pyrolysis, with results suggesting severe torrefaction parameters may be detrimental to aromatic yields and coke formation. [32,33] For non-catalytic pyrolysis with torrefaction as a pretreatment, the trend is for a lower oxygen content in the pretreated product at the cost of lower total yield. Torrefaction yields bio-oil with lower oxygen content, lower water content, higher pH, and higher heating value [30, 32, 33]. The primary goal of this research will be to provide data to present the potential advantages of using torrefaction and red mud to treat pyrolysis oil before downstream modifications. Additionally, water washing of the biomass feedstock will be implemented to reduce the ash content, and subsequent testing will determine the effect of ash reduction on pyrolysis oils.

Specific Objectives

1. To investigate the impacts of ash reduction via water washing on the yield and quality characteristics of fast pyrolysis bio-oil produced from Napier Grass

2. To study the effects of torrefaction of water washed feedstocks on the yield and quality characteristics of fast pyrolysis bio-oil

3. To determine the effects, and efficacy, of using red mud as the bed material for in-situ catalytic fast pyrolysis.

Chapter 2

Background and Literature Review

2.1 Lignocellulosic Biomass

Biomass consists of organic sources of materials derived either from plant or animal matter. A subset of biomass, lignocellulosic biomass consists of plant matter with a composition of lignin, cellulose, and hemicellulose. Cellulose is the simplest of the three, being a polysaccharide of β 1,4 D-glucose units. Hemicellulose is a branched polysaccharide which can be comprised of xyloglucan, glucuronoxylan, arabinoxylan, glucomannan, and galactomannan. A 4th component, pectin, is a complex polysaccharide containing 1,4 linked α-D-galacturonic acid that is found in both the primary and secondary cell walls. Lignin adds structural strength to the secondary cell wall and is a phenol polymer [34].

2.1.1 Woody and Non-Woody Materials

Within lignocellulosic biomass, a further distinction can be established between woody and non-woody feedstocks. Woody materials can be considered trees, or any parts of trees that result from cultivation, harvesting, or processing. Non-woody feedstocks are typically perennial grasses, other non-food crops, and agricultural residues e.g. corn stover. Some

species, such as sugar cane, have been genetically modified to produce more lignocellulosic biomass for bioenergy production and are referred to as 'energy crops'. Compositionally, woody materials tend to have higher lignin and hemicellulose content and have lower cellulose crystallinity than non-woody materials [35].

Within non-woody crops, a further distinction exists between C3 and C4 plants. C4 plants, such as elephant grass, are more efficient at photosynthesis than their C3 counterparts due to structural differences in the plant. Elephant grass, in particular, has yields reported in the range of 30-40 dry tons/ha/yr [9–11].

2.2 Preprocessing and Pretreatment of Biomass

2.2.1 Reduction of Inorganic Content

Inorganic content, or ash, composes a relatively small fraction of biomass makeup; less than 5% for the supplied Napier grass, with pine typically reported under 1%. However, it can have appreciable effects on the pyrolysis process, particularly the alkali metals. These effects have been studied in previous works, commonly using some form of 'demineralization' via water or acid leaching. Reduction in the ash content has been shown to improve the yield of organics while decreasing moisture content in regards to fast pyrolysis liquids. Additionally, ash can lead to the formation of coke during upgrading steps. [36–40]

2.2.2 Torrefaction

Torrefaction is a thermal pretreatment technology, sometimes referred to as a 'mild pyrolysis,' carried out in an inert atmosphere. It has a longer residence time, typically between 10 and 60 minutes, and is carried out at a relatively lower temperature, usually 200-300°C. This process converts biomass feedstock into an often brown or blackened stock, a result of the biomass

carbonizing, that is dried during the process. Some water is regained from humidity after the process, but overall the stock has a much lower affinity for moisture. This dried feedstock is then mechanically favorable to feed systems which can be sensitive to moisture. Additionally, torrefied biomass becomes brittle and has a lower energy requirement for grinding. This reduction varies by torrefaction parameters and feedstock, but as an example, pine chips were reported to have 10 times less specific grinding energy when torrefied at 300°C for 30 minute residence time [41]. Torrefaction also increases the C:H ratio by the evolution of oxygen containing compounds. The result of this effect is a tradeoff of higher energy density in the torrefied biomass and mass loss during the process [13, 42]. Much of the mass loss can be attributed to the evolution of carbon monoxide and carbon dioxide. However, some of the mass loss is the result of organic acids, such as acetic acid due to hemicellulose decomposition [13, 36, 43, 44].

Effects on Biomass Types

Torrefaction has received some attention as a possible pretreatment for pyrolysis, with several studies having been conducted on woody products to date. In a study on Douglas Fir using a microwave pyrolysis unit [45], bio-oil yields ranged from 17.14-40.25 wt% compared to raw biomass pyrolysis yields of 53.42 wt%. Biochar and syngas yields were improved, ranging from 31.13-49.61 wt% and 24.13-34.37 wt% respectively, compared with raw biomass yields of 27.1 wt% and 19.48 wt% respectively. Also noteworthy from the study where the significant changes to syngas composition. The raw biomass produced approximately 26% (v/v) of carbon dioxide, 44% (v/v) carbon monoxide, 6% (v/v) methane, and 5% (v/v) hydrocarbons. Torrefaction affected the carbon monoxide content varying from 25.95- 45.30% (v/v), while carbon dioxide ranged from 8.75-18.18% (v/v). Methane content rose to 10.99-25.54% (v/v), and hydrogen was detected between 2.38-20.61% (v/v) [45]. Torrefaction effects are primarily influenced by the reaction temperature, with residence times secondarily affecting the process

by allowing an amount of biomass to be affected by this temperature. As such, higher temperatures and longer residence times, e.g. 300°C for 30 minutes, are considered harsher treatments. These severe torrefaction processes result in a higher mass loss and increasing HHV as shown in many studies [13].

Meng et al. studied fast pyrolysis of Loblolly Pine in a fluidized bed reactor and found a decrease in the oxygen/carbon ratio from .63 in the raw sample to a range of .52-.31 depending on torrefaction parameters [30]. As the torrefaction temperature and time increased, the HHV of the feedstock increased, while the mass loss increased, causing an increase in the energy density of the material. This shift in the O:C and H:C ratios lead to a change in the biomass feedstock gravitating to a more coal-like composition. In the same study [30], the O:C ratio was decreased from .63 to .31 by torrefaction of Loblolly Pine at 330 °C for 2.5 minutes. This same treatment resulted in the HHV increasing from 20.0 to 26.3 dry based MJ/kg. Fast pyrolysis of the torrefied pine showed a higher quantity of pyrolytic lignin compounds and reduced overall oil yield, however, the oil produced showed lower O:C ratios and moisture content.

2.3 Pyrolysis Reaction and Mechanism

Pyrolysis is a thermochemical process carried out in the absence of oxygen at temperatures usually ranging from 400-600 °C. During the process, biomass is broken down into bio-oil, bio-char, and syngas. Fluidized bed pyrolysis is one of the common forms of pyrolysis; however, it is not the only reactor capable of carrying out the process. Bio-oils generated by pyrolysis are high in carbon while being low in nitrogen and sulfur. The oil generated by the pyrolysis process is considered to be of a much lower quality than crude petroleum oil. Table 2.1 lists typical parameters of bio-oil properties. It consists of fragmented and depolymerized cell wall matter, and as such, has a different chemical composition. Also, it generally has

Table 2.1: Typical values of pyrolysis and crude oil parameters.

Properties	Fast pyrolysis oil from wood [16]	Heavy petroleum oil [15]
Moisture Content (%)	25	0.1
pH	2.5	-
HHV (MJ/kg)	17	40
Oxygen Content (%)	38	1.0
Ash (%)	0.1	0.1

a much higher water content (15-30 wt% vs. .1 wt%) and oxygen content (35-40 wt% vs. 1 wt%) than crude oil. These factors contribute to pyrolysis oil having roughly half the heating value of crude oil. The pH of bio-oils tends to be between 2-3, which makes them unstable as well as gives them storage issues and requires upgrades before further usage. Ash content in the bio-oils can cause problems when used in engines as well as present issues with corrosion [22]. Biomass fast pyrolysis has several essential features which include:

- the complete absence of oxygen during conversion to prevent combustion;
- the high rate of heat transfer, which further demands high temperatures and smaller particle sizes;
- the reaction temperature of 500°C with low residence times to foster higher liquid yields and reduce the chance of secondary reactions;
- quenching of pyrolysis vapors to condense into bio-oil, and again reduce the chance of secondary reactions.

2.4 Catalytic Pyrolysis

One of the treatment options for upgrading bio-oil is catalytic cracking of the pyrolysis vapors with the goal of lowering the oxygen content and breaking large aromatics into smaller

structures. Catalytic fast pyrolysis has potential advantages over hydrocracking in that catalytic cracking of pyrolysis vapors does not require hydrogen, pressurization, or in some cases, additional heating. This process is not without drawbacks related to the catalyst. Coking and deactivation of the catalyst require that the catalyst is replaced or regenerated to maintain optimum efficiency. Catalytic pyrolysis also leads to lower liquids yield as some of the molecules are broken into lighter weight components that fail to condense [46]. For in-situ catalysts as used in this study's system, sintering resistance must be considered due to reaction temperature.

2.4.1 Catalysts

Zeolite catalyst, such as ZSM-5, are aluminosilicates. Catalytic cracking can decrease the oxygen content of oils by concurrent dehydration, decarboxylation, and decarbonylation in the presence of a zeolite catalyst [47]. ZSM-5 has largely been used over other zeolites due to its cracking abilities. Zeolites are also used in the petroleum industry, and many studies can be found on the subject [46]. For the design of the pyrolysis reactor in this study, catalyst temperature and pyrolysis temperature cannot be separated. Zeolites tend to show higher activity in temperature ranges under 500°C. With this constraint, other catalyst options will be explored due to the operating temperature being 500°C or higher.

Mixed metal oxides present another form of available catalyst. For the purpose of this research, the noble metal catalyst will be considered economically prohibitive. Other metal oxides have been investigated for their potential as an upgrading catalyst. The effects of such catalyst vary by metal used and reactor parameters. In an analytical study of nano metal oxides, Fe_2O_3 formed hydrocarbons, and CaO caused a reduction in phenols as well as eliminating acids [48].

Red mud, another option for mixed metal oxide catalysts, is a waste product in the aluminum production process from bauxite refinement, and it is a combination of several

metal oxides. It is considered hazardous due to its high alkalinity. Among others, this compound can include Fe_2O_3, Al_2O_3, SiO_2 and CaO, which contains a mixture of the previously mentioned catalysts. Red mud offers a cheap, disposable catalyst option with potential to catalyze favorable changes to the bio-oil composition. Its abundance and low cost make it an attractive option as a catalyst. Work by Yathavan et al. [29] has shown red mud to be catalytically active for the reduction of levoglucosan as well as oxygenated groups and acids while increasing the output of aromatic compounds. A further study by Agblevor et al. [49] tested catalytic pyrolysis with a red mud catalyst and hydro-treating of the liquid product after that. The study found similarly promising results for red mud as a catalyst, producing lower oxygen content (values between 20-25%) oils.

2.5 Pyrolysis Reactors

2.5.1 Continuous Fluidized Bed

A circulating fluidized bed (CFB) is a configuration in which hot sand is circulated within the reactor and transfers heat to the biomass before being reheated itself. CFBs have been well established and are already in use in the petroleum industry at high throughputs [24,50]. Liquid yields of up to 60-80 wt% (wet basis) have been reported for fast pyrolysis [14,24,51]. Biochar and syngas production from the process can be used within the process itself or externally such that fast pyrolysis does not have to have a dedicated waste stream. To achieve low residence times, typically less than 2 seconds, a smaller particle size is required. For the conversion of biomass to liquids, a particle size of 3-6 mm or less is considered desirable. Additionally, the reactor will require a carrier gas, such as nitrogen, for fluidization [14,24,52]. Much of the work done on biomass conversion has been carried out on woody products where the literature tends to favor 500°C reaction temperatures [14,53]. This reaction temperature typically results in the highest product yield for those feedstocks. This paper will employ the

usage of a bubbling fluidized bed reactor. In this design, pyrolysis vapors are not circulated back through the sand bed. Vapors follow a linear stream to the exit line, and the sand bed is fluidized to the point of generating bubbles that provide movement, yet is calm enough that mass will not be lost from the bed over time.

Of a slightly different design is the bubbling fluidized bed (BFB). This reactor is built in the same fashion with one key exception - the vapors are processed in a linear path, and there is no recirculation back through the sand bed. This setup can operate under all the same parameters as a CFB; however, better results are obtained from a smaller particle size of 2 mm or less [16].

2.6 Parameters Impacting Pyrolysis Products

2.6.1 Compositions

Cellulose and hemicellulose are degraded under pyrolysis conditions; however, lignin is more thermally resistant. As a result, higher lignin content favors higher char yields [54]. Cellulose and hemicellulose degrade to give off acetic acid, formic acid, water, and volatile compounds [55].

2.6.2 Presence of Inorganics

Ash, in particular, alkali metals and alkali earth metal, can have catalytic effects during fast pyrolysis. While research has found hot gas filtration to reduce the ash present in pyrolysis oils, these ash materials can cause reactions before separation that preferentially alter vapors towards char and non-condensable gas production, thus lowering liquid yields [54]. Alkali and alkaline earth metals have been shown to adversely effect the liquid production of the pyrolysis process granting lower liquid yields and higher char yields [40, 56, 57].

2.6.3 Pretreatment

While genetic modifications hope to provide biomass that is less recalcitrant to chemical conversions, thermal conversion is able to bypass several of the inherent issues with biomass. Additionally, some steps can be taken to improve thermal conversion rates. In the case of fast pyrolysis, any moisture that is present in the feedstock will transport into the liquid product. To counter this, feedstock drying to 10% or lower is typically carried out to improve oil quality. To obtain good heat transfer, feedstock must be ground to a small particle size [51, 52]. While these steps may seem minor, they are important considerations for overall energy balances and costs concerns [24].

Torrefied biomass has some properties that make it an attractive possibility as a pretreatment for pyrolysis. Torrefied biomass is hydrophobic, maintaining a naturally lower moisture rate. This improves stability and durability aiding with transportation and storage. Additionally, torrefied biomass is brittle and, thanks in part to the low moisture content, is easier to grind. This improved grindability of biomass could offset preparation costs at the mill. Chemically the torrefied biomass has a lower O:C ratio which may aide in reducing oxygen content in bio-oil produced downstream. A cost-benefit scheme will have to be arranged to determine if the extra energy cost and mass loss during torrefaction merit its use based on the downstream benefits [13]. Of the three temperatures tested in [30], 270, 300, and 330 degrees Celsius, all showed an increase in pyrolytic lignin. This is believed to be due to the breakdown of cellulose and hemicellulose during the torrefaction process. The downside to the potential upgrades brought by torrefaction is the decrease in oil yields, from 67.2% untorrefied to 33.5% for the harshest pretreatment. A different study [58] showed that torrefaction decreased oil yields using treatments at 100, 225, 250, and 275 °C each for 20 minute holding times. 100°C treated mass generated 22.4% w/w oil vs. only 11.0% at 275. Gas production in showed a sharp decrease at 275 °C down to 22.4% vs. 56.6% in the 100°C sample, and likewise a large increase in char production; 66.5% vs. 21.0% respectively. Work

done by Boateng et al. [59] involved switchgrass and hardwood pellets using torrefaction as a pretreatment to fast pyrolysis. In particular, switchgrass was torrefied for 1.5 hours at 250 °C before pyrolysis. Liquids yield in fast pyrolysis decreased by 6.5%, O:C ratio went down by .8 to .40, and the HHV increased from 19.4 to 22.8 MJ/kg. Acidity was measured by total acidity number (TAN) which reduced from 117 to 85 mg KOH/g.

2.6.4 Temperature

Much of the literature seems to agree on 500 °C being the optimum temperature for fast pyrolysis. Work by Bridgewater et al. shows the highest yield of organics near this temperature [14]. This is believed to be high enough of a temperature to breakdown biomass without being so high as to crack the pyrolysis vapors into non-condensable gases or polymerizing into char. Temperature and time are key variables to control when trying to maximize yields and minimize co-products.

2.6.5 Residence Time, Particle Size, and Carrier Gas

In general, residence times should be kept short; under 5 seconds. Residence time is a delicate balance between too short - not fully deconstructing lignin, and too long - causing secondary reactions that adversely affect the products [14].

Small particle sizes are essential for rapid heat transfer and complete pyrolysis. Typical sizes on the order of 3-6 mm are acceptable for CFBs; however, for fluid beds smaller sizes, i.e. less than 2 mm, are more desirable [14].

The carrier gas of choice for these experiments will be nitrogen. The fluidized bed reactor is such that an inert carrier gas is required for mobilization of the sand bed, transportation of the pyrolysis vapors, and prevention of combustion. These two requirements dictate such a flow rate that any oxygen present upon start up is flushed from the system, and the

continuous feeding of inert carrier gas prevents any combustion of the products from taking place.

2.7 Summary

Fast pyrolysis provides a viable conversion pathway to produce liquid fuels from solid feedstocks. However, low quality prevents this bio-crude from being a 'drop-in' product to existing infrastructure. Alkali metals can degrade pyrolysis vapors operating as an in-situ catalyst; therefore their removal or reduction is desirable. Water washing of feedstocks can provide this reduction. Additionally, removal of organic acid precursors in the form of hemicellulose and cellulose can improve quality by increasing pH while decreasing oxygen content. To achieve this, torrefaction is performed on the feedstocks as an additional pre-treatment. Catalytic reactions can further attenuate acid and oxygenate production, and for this reason, red mud is used. To minimize modifications to the fast pyrolysis system, the catalyst is used in-situ as the bed material.

Chapter 3

Methods and Materials

3.1 Materials

Feedstock

Napier grass and energy cane samples were obtained from the experimental farm at the Fort Valley State University, Fort Valley, GA. Harvested samples were size reduced using a hammer mill with 1/2" screen size. All biomass were stored in plastic containers at room temperature. Napier grass samples were harvested in 2013 and 2014 and were mixed in a 50/50 ratio to provide a single mixed feedstock for further processing. The initial mean moisture content of the samples range from 2-10% (wet basis). The initial mean ash content of the feedstocks has a range of 2.7-4.6% (dry basis).

Water Washing

A subsample of Napier grass was treated by water washing to reduce inorganic ash content of the biomass. The water washing protocol was developed in an attempt to reduce the Napier grass ash content and was fixed at a ratio of 25 g mass per 1L of DI water and soaked for 2 hours. After soaking, a 150 µm screen was used to separate the biomass from the water. The

biomass was then placed in a furnace at 105°C for at least 20 hours to dry. Water washed samples were completed in 1500 g batches.

3.2 Torrefaction

Reactor Configuration and Operations

Torrefaction was carried out in a batch operation completed in a furnace (Type 30400 Thermolyne, Barnstead International, USA). Figure 3.1 shows the process flow diagram for the setup. Ground biomass was added to the vessel which was then sealed with a graphite gasket and a series of 45 screws along the perimeter of the flange. The vessel has an inlet and outlet source for nitrogen and vapor flow. Nitrogen was fed through the vessel at a rate of approximately 1-1.5 liters per minute, which passes through the heating material and into the condenser assembly. The condenser apparatus consists of 4 canisters submerged in an

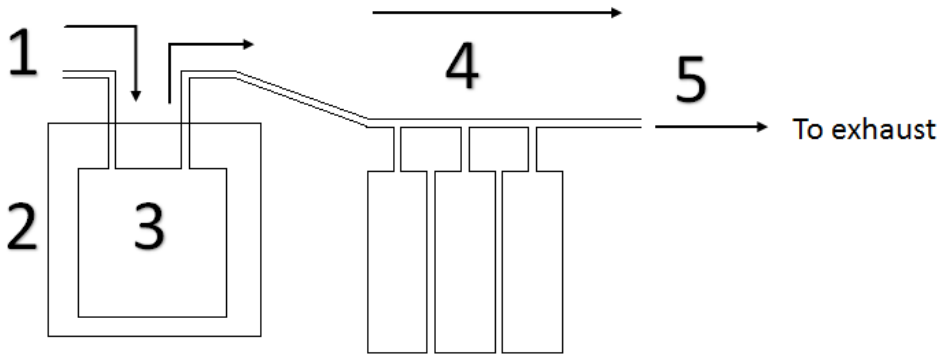

Figure 3.1: Torrefaction Batch Reactor: 1) Gas inlet, 2) furnace, 3) Feedstock vessel, 4) Liquid Condensers (in ice bath), 5) NCG exhaust

ice water bath to within 1 inch of the top of the canister. Non-condensible gases were then exhausted from the exit port. The temperature was slowly ramped up to the target value, where it was maintained for the desired residence time. After completion of the process, the

furnace door was opened to allow for rapid cooling of the vessel. Upon cooling, the nitrogen gas was shut off and the vessel was removed. The torrefied materials were weighed and stored in plastic containers, with subsamples being kept in Ziploc bags. The condenser assembly was harvested into glass bottles that were subsequently stored in a 2°C refrigerator.

Torrefaction was carried out at two temperatures, 250°C and 275°C, using residence times of 30 minutes each. Each run consisted of 1 kg of 1/2" ground material being loaded to the vessel. The vessel was loaded in the furnace and connected to the inlet line and condenser assembly, which was further connected to the exhaust line. Heating was provided by the furnace. Biomass was allowed to reach the target temperature before a timer was started for residence time. During residence time, the sample was controlled within 2% of the target temperature. After the residence time has been reached, the furnace was shut off and the door was opened to facilitate cooling. A box fan was aimed at the vessel to further increase the cooling rate. Each temperature was completed multiple times to provide multiple replications of each material and enough torrefied feedstock to operate the fluidized reactor. Mass yield balance and characterization of the solid mass were completed in addition to BFB product analysis.

3.3 Fast Pyrolysis

Material Preparation

Biomass was ground through a 1/16" screen via hammer milling and dried in an oven (FD 115 - UL, Binder, Germany) at 105°C before being loaded in the BFB reactor hopper. Sand was dried at 550°C in a muffler furnace (Thermo Scientific, Waltham, MA) that was allowed passive air flow. This process was repeated as necessary between runs to regenerate sand for fluidization of later trials.

Red Mud was acquired for a previous study from Tio Tinto (Alcan, Canada). The

wet slurry was oven dried at 105°C overnight. The dried product was crushed mortar and pestle to approximately 1" diameter or smaller rocks. The red mud was then loaded into the torrefaction apparatus and heat treated to 500°C. Nitrogen gas was passed through the material to remove moisture content and maintain 'reactor like' operating parameters. This was done to mimic pyrolysis conditions and prevent potential reactions and alterations to the material due to the presence of oxygen at high temperatures. The heat treated material was then ground with mortar and pestle, with the material then passed through -20+30 mesh sieves, and over-sized particles being reground to size. The sample was then stored in a sealed glass container to maintain low moisture content until usage. Sub-samples of each batch were collected.

Raw red mud compositional analysis (provided by Justin Weber, Dr. James Kastner) was previously conducted, and relevant data is show in Table 3.1. Of particular note is the high presence of iron (22.6%), sodium (14.5%), and aluminum (14.4%), with lower levels of silicon, calcium, and titanium (8.6%, 4.4%, and 4.4% respectively).

Table 3.1: Compositional analysis of Red Mud, raw

Metal	**Red Mud, untreated**
	% mass (dry basis)
Fe	22.6
Na	14.5
Al	14.4
Si	8.6
Ca	4.4
Ti	4.4

Reactor Configuration

The BFB reactor's basic design was shown in Figure 3.2. It has two inlet ports; one for gas and one for feedstock. These lines converge at the sand bed. The carrier gas was fed through the lower-back port of the reactor and passes through a preheating zone. This section of

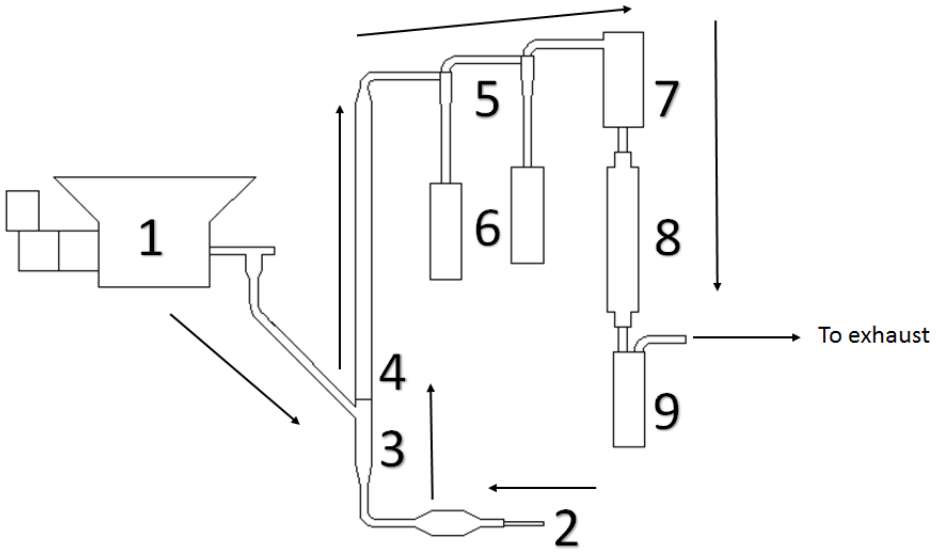

Figure 3.2: Bubbling Fluidized Bed Reactor: 1) Feedstock hopper, 2) Nitrogen inlet and pre-heater, 3)Sand Bed, 4) Riser Column, 5) Solid separation cyclones, 6) Solid collections, 7) Hot gas filter, 8) Condenser, 9) Liquid collections and exhausting of NCGs.

the reactor was a packed bed with a mix of alumina and stainless steel beads to speed the heating of the gas as it was passed through. The gas was then passed through an aeration plate to evenly distribute the gas as it entered into the sand bed.

The feedstock was loaded into the hopper until the hopper reaches between approximately 1/2 to 3/4 capacity, by volume, as this tends to favor a more even mass flow rate. Within the hopper was an auger powered by an electric motor. The auger carries feedstock horizontally to a drop tube where the feedstock was then gravity fed to the fluidized bed.

The fluidized bed was loaded pre-run with 250 g of sand or 175 g of catalyst. The feedstock inlet entered into the side of the sand bed approximately 1/4 the height of the sand bed from the aeration plate. The fluid action of the sand bed acted to draw in feedstock and begin the pyrolysis process. As the breakdown occurred, mass loss caused the solid char to be carried

up through the riser column along with the pyrolysis vapors. This mixture then entered a solid cyclone where a majority of solids were deposited. For the vapor and remaining solids, the next step was an additional solid cyclone. After this, the pyrolysis vapors typically saw a 99% reduction in solids content. After the second solid cyclone, a final solid separation step was completed via hot gas filtration with a 40 µm screen size (Purolator Facet, Inc., North Carolina, USA). The vapors were then passed through a shell and tube condenser, which was crafted using a stainless steel housing with 1/4" copper tubing coiled inside. The coils were wrapped around three times to maximize surface area. The condenser was maintained by a water hose in a single pass, with tap water coming in to the condenser, and exiting through another hose to the nearby woods. At the bottom of each solid cyclone, and the condenser, were stainless steel containers. For the liquids container, a special connection was attached that allowed the liquids and vapors to enter, and the remaining vapors to escape. These vapors then passed through a 3-container, sequential, water bath that was maintained below 0°C. Typical temperatures for the water bath were below -10°C. The NCGs then exited the building through an exhaust line.

All zones were heated to 500°C, except the hot gas filter, which was set to 450 °C, with temperature regulations at the appointed zones and temperatures maintained ± 2%. The sand bed was loaded with the appropriate mass of sand or catalyst. Upon nearing operating temperatures, nitrogen gas was fed through the system at a rate of 19-22 liters per minute for sand runs, or 21-24 liters per minute for catalyst runs. The reactor was then allowed to reach thermal equilibrium before initiating the feed system. The feeder was operated after equilibrium was reached, and it was allowed to run for a length of time - typically 30-60 minutes. Upon completion of the run, the feed line was shut down, and nitrogen was allowed to flow through the system for an additional 30 minutes at operating temperature to move any remaining pyrolysis vapors through the system. The system was then allowed to cool under inert conditions, after which all canisters were removed. All masses were measured

and stored as with torrefaction. Additionally, the fluid bed was purged from the reactor. For sand, this mass was then placed in a crucible and heated in a furnace to 500°C. Sub-samples of both bed types were taken after each run. Sand, after burning for cleaning, was reused in subsequent runs, while red mud was stored for further analysis. The condenser was processed using TAM, toluene, acetone, methanol in a 1:1:1 ratio. 600 mL of TAM was loaded in to the condenser, which was sealed at both end, mixed, and allowed to sit for typically 1 hour. Afterward, the sample was removed and stored in a glass bottle at 2°C. This served to harvest samples contained within the condenser, as well as to clean the condenser before the next run. The reactor was assumed to have minimal residual mass after this, and, as such, the production of NCGs were assumed to be the difference in mass processed and mass collected. Torrefied and base feedstocks were pyrolyzed with a catalytic bed to determine the effects of torrefaction on catalyst coking. Each BFB run was duplicated to provide a statistical replication and ensure repeatability.

3.4 Experimental Plan

Figure 3.3 shows a summary flowchart of Napier grass treatments. A control group was taken at each level. A group of water-washed samples were kept as a control against the torrefied groups. Torrefaction was only tested post-water wash. Each experiment was conducted for two replications. More reps were reserved for use as required to sort out a high variability between the initial two reps, or as necessitated to generate enough material for a downstream experiment (e.g. as many torrefaction runs as were necessary to run the BFB). Statistical analysis was manually programmed into Excel.

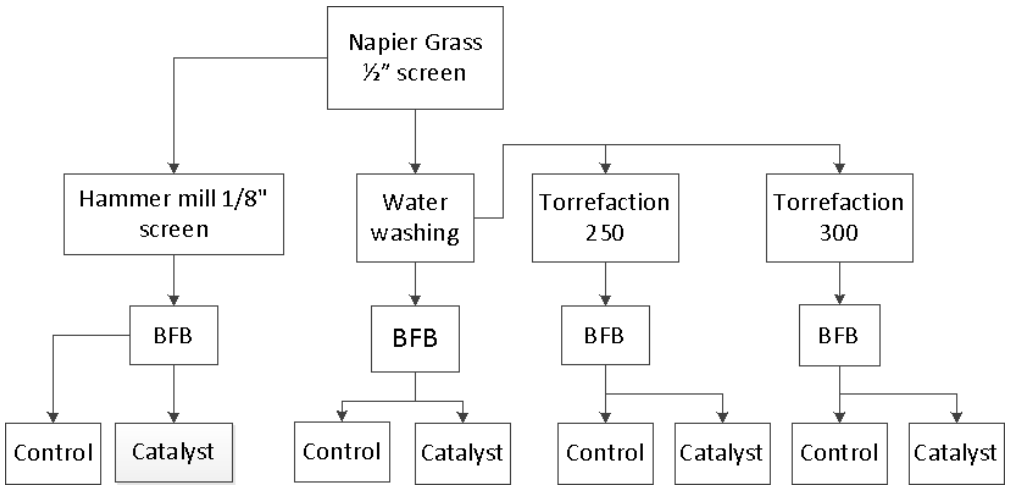

Figure 3.3: Flowchart of Napier grass processing

3.5 Analytical Methods

3.5.1 Biomass Physical Properties

The bulk density of the feedstock was obtained by first taking the weight of a container. Within the container was a fill line marking a known volume. The container was filled to the marking and tapped ten times on a solid platform. Biomass was added until reaching the mark when leveled, and the mass of the container taken again. The mass:volume ratio was then used to derive density.

Particle size distribution was determined by sifting dried biomass through a series of sieves (the exact series varied depending on bulk vs. ground materials). The mass of each sieve was noted before assembly. Biomass was then loaded in the top, largest opening of the sieves, and a lid was placed over the assembly. The series was shaken by a sieve shaker for 10 minutes set to 60 amplitude (Model AS 200, Retsch, Germany). Each mass was then recorded to determine the particle size distribution by a mass basis. A catch pan was attached to the bottom of the sieve assembly to catch the smallest of particles.

3.5.2 Proximate Analysis

Proximate analysis was conducted on a thermogravimetric analyzer (TGA701, LECO, USA). 1-2 g of the sample were loaded into a crucible and processed by ASTM method D5142 programed to determine moisture, volatile, ash, and fixed carbon content. Values were determined by changes in mass over time as a function of temperature increase and presence or absence of oxygen.

3.5.3 Ultimate Analysis

Ultimate analysis was conducted using a CHNS analyzer (FLASH 2000 CHNS analyzer, Thermo Scientific, USA) with oxygen being calculated as the assumed difference.

3.5.4 Mineral Analysis

Mineral analysis of the feedstock material was conducted by the Feed and Environmental Water Laboratory at The University of Georgia.

3.5.5 Higher Heating Value

Bomb calorimetry (C2000 basic with KV 600 digital, IKA, Germany) was used for the determination of higher heating value.

3.5.6 Moisture Content

It was desired to use Karl Fischer titration (DL31, Mettler Toledo, USA) to determine the moisture content of the generated liquids. As with the CHNS analysis, the instrument is in need of repair and samples were not able to be processed. Sub-sampling was done to allow these samples to be tested should the repairs become available, and the remaining liquids processed for further data collection.

The moisture content of the ground solids was provided by proximate analysis, while the moisture content of the base feedstock was determined by oven dried mass difference. Measured samples were loaded into a 105°C furnace and mass was recorded at 24-hour intervals until the reading was consistent.

3.5.7 Oil Yield and Further Analyses

For the liquids collected from the condenser, GC-MS analysis was carried out to qualitatively identify compounds contained therein. The remaining liquids, having been combined to one unit, were separated using Dichloromethane (DCM). This separation produced a polar fraction, and a, theoretically, nearly water-free non-polar fraction. These fractions were filter through 45 µm nylon syringe filters before being analyzed by HPLC and GC-MS respectively.

HPLC analysis was carried out on a SHIMADZU LC-20 AT (SHIMADZU, Japan) equipped with a RID-10A and Coregel 64 H column. This provided quantifiable data on organic acids and sugars, as well as Furfural and 5HMF. GC-MS analysis(6890 GC, HP, USA, coupled with 5973 MSD, HP, USA), equipped with a CIS 4 inlet (Gerstel, Germany), of the non-polar sample was done on an HP-5 MS capillary column.

Preliminary data was available for the energy cane control run. DCM fractions were processed with an initial oven temperature of 50°C with no hold time, 7°C/min to 100°C, which was held for 1 minute, followed by 12°C/min heating ramp to 275°C, which was held for 3 minutes. TAM fractions were processed with 45°C initial temperature with no holding time, 10.50°C heating ramp to 275°C which was held for 3 minutes. Both samples had the same gas flow, inlet temperature and injection volume. Carrier gas flow was set to 2 mL/min; the inlet temperature was 250°C, and 0.5 µm of the sample was injected.

Coke formation was determined by burning of bed material, using the mass loss as the value of coke. Sand, from non-catalytic runs, was burned in full to generate mass for the next run. RMC was collected and stored. Duplicate samples of RMC were burned to test

for coke formation.

Statistical Analyses

Statistical analysis of various parameters was processed by Analysis of Variance (ANOVA). The data was broken into two main fractions: effects of physical pre-treatment via water washing, and effects of thermal treatment via torrefaction. For the torrefaction section, the water washed sample serves as the control group. Within these sections, there is a treatment option for the presence or absence of catalyst. With this design, the ANOVA were programmed as factorial designs of fixed effect parameters. Raw data values were used to construct totals, which were used for the sums of squares calculations. Mean square values were divided by the error mean square to produce F values. All calculations and statistics were manually programmed into Excel. The only built-in functions used in Excel were for the mean (AVERAGE), standard deviation (STDEV.S), and sums of squares (SUMSQ). Templates were built and tested using alternate data with known solutions for debugging of the table. The results are located in Appendix B.

Water washing is not expected to have a large significance on the liquid yield, but a strong effect on the product distribution in that yield. Torrefaction, alternatively, is expected to have an effect on both liquid yields, and product distribution within those yields. The presence of the catalyst is expected to have a significant impact on the yield distribution and product distribution.

Chapter 4

Results and Discussion

For the purposes of this chapter, the water washed group will be referred to as Water Wash or WW, the 250°C and 275°C torrefaction groups will be referred to as T250 and T275 respectively. It is worth repeating that both torrefaction groups were carried out using water washed feedstocks. All values are reported as mean value (with standard deviation in parenthesis) unless otherwise noted. Lastly, any data not acquired is marked N/A (this is not the same as not detected).

4.1 Physical Properties and Chemical Compositions

The results of physical property analysis are displayed in Table 4.1. The oven dried moisture content was derived after allowing samples to sit in their respective container for approximately 3 months. As was expected, available volatile content decreased with increasing torrefaction severity. Mean ash content for water washed samples decreased by 37.2%, indication the process as functioning, with room for improvement. Carbon content shows steadying increase across torrefaction groups, rising from 45% in the water wash control group to 57% in the T275 group. The T275 value is a single test from an outside lab. This

Table 4.1: Physical properties of feedstock materials

Physical Properties	Energy Cane	Elephant Grass	WW	T250	T275
Moisture (%)	10.06 (0.12)	9.55 (0.08)	4.48 (0.34)	N/A	N/A
Proximate Analysis (%, dry basis)					
Moisture	8.28 (0.06)	7.92 (0.04)	5.11 (1.58)	2.76 (0.78)	4.81 (0.18)
Volatile	77.85 (0.68)	76.98 (0.92)	80.18 (0.59)	74.24 (1.38)	61.29 (6.58)
Ash	3.99 (0.19)	4.46 (0.31)	2.80 (0.45)	2.74 (0.35)	4.49 (1.21)
Fixed Carbon	18.16 (0.74)	18.52 (0.63)	17.02 (0.54)	23.06 (1.24)	34.22 (5.39)
Ultimate Analysis (%, wet basis)					
N	0.59 (0.05)	0.80 (0.02)	0.60 (0.15)	0.58 (0.12)	N/A
C	44.40 (0.05)	43.61 (0.14)	45.39 (0.59)	52.48 (0.44)	57.616*
H	6.23 (0.02)	5.89 (0.15)	5.88 (0.05)	5.72 (0.05)	N/A
S	0.00 (0.00)	0.00 (0.00)	0.00 (0.00)	0.00 (0.00)	N/A
O (assumed difference)	48.78 (0.07)	49.70 (0.02)	48.14 (0.46)	41.23 (0.38)	N/A
Higher Heating Value (MJ/kg)	17.96 (0.61)	18.17 (0.22)	18.98 (1.36)	20.27 (1.29)	N/A

was discussed in the methods section, and it is assumed to be reasonably representative based on the low standard deviation of our own tests. Alongside carbon increase, torrefaction showed a decreased oxygen value in the T250 group, and the trend is expected to continue with the T275 group, with oxygen content expected to drop below 40%.

Particle size distribution and bulk density data are presented in Tables 4.2, and 4.3. Particle size distributions followed expectations, with torrefaction having negligible impacts. Bulk density decreased due to water washing, which is explained by the lower moisture content of that sample. Further dehydration and volatilization of material in the T275 further decreased bulk density of the feedstocks. Figure 4.1 shows the graphical trend, with what appears to be a bimodal distribution across all groups. As seen in Figure 4.2, over 50% of the material for all groups is less than than 2 mm.

Table 4.2: Particle size distribution of all feedstocks, chopped

Particle Size Distribution (% mass)	Energy Cane	Elephant Grass	WW	T250	T275
4.00 mm	35.28 (34.70)	6.32 (0.04)	4.91 (0.74)	3.74 (0.50)	3.83 (0.07)
2.80 mm	11.04 (9.01)	20.65 (0.32)	16.90 (2.54)	15.49 (2.50)	15.23 (0.88)
2.00 mm	14.43 (10.81)	27.08 (1.63)	22.57 (3.07)	22.69 (2.19)	28.58 (8.72)
1.60 mm	8.14 (5.71)	10.01 (1.11)	11.65 (1.87)	12.69 (1.34)	10.47 (5.77)
1.25 mm	7.19 (3.36)	9.87 (0.13)	8.95 (0.72)	10.97 (1.04)	10.57 (1.00)
500 µm	16.44 (4.91)	18.38 (0.81)	21.90 (1.23)	23.62 (2.59)	20.52 (2.91)
<500 µm	7.42 (2.24)	7.59 (2.12)	13.15 (5.66)	11.39 (2.87)	10.65 (1.01)

Table 4.3: Bulk density of feedstocks

Bulk Density (kg/m3)	Energy Cane	Elephant Grass	WW	T250	T275
Chopped	97.96 (4.24)	110.80 (2.19)	97.58 (2.67)	98.47 (3.35)	90.60 (2.58)
Ground	190.92 (1.24)	220.21 (4.17)	218.19 (2.27)	230.76 (2.41)	243.19 (4.33)

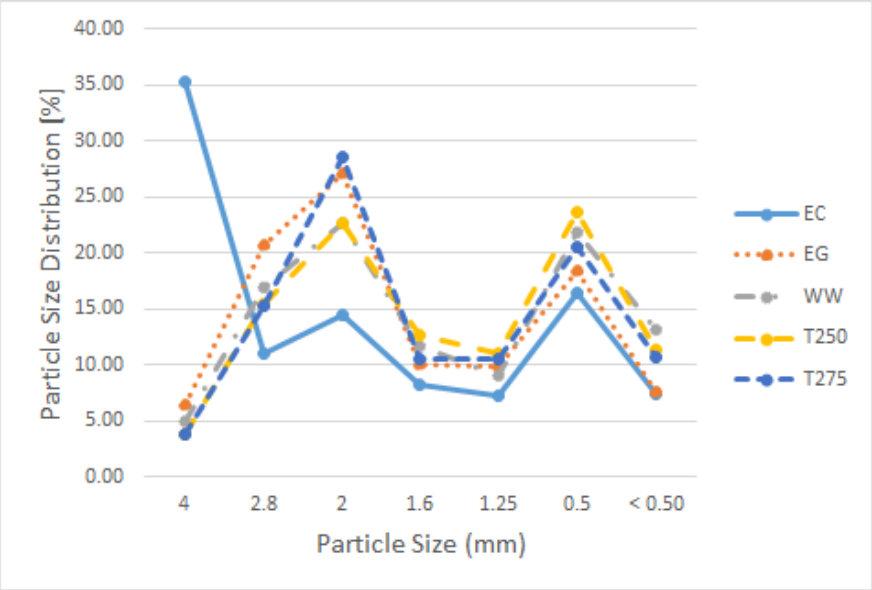

Figure 4.1: Particle size distribution of 1/2" feedstock

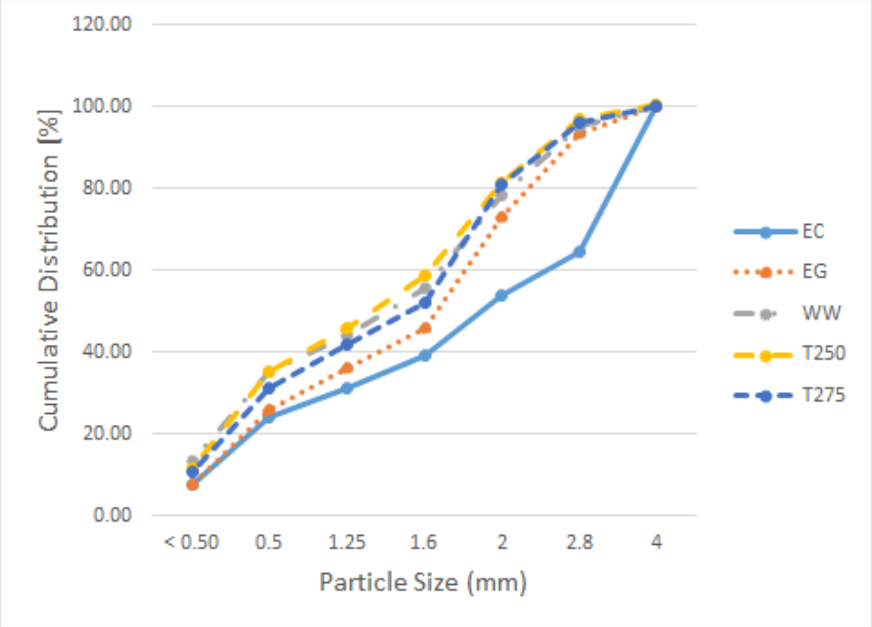

Figure 4.2: Cumulative passing graph for 1/2" feedstock

4.1.1 Water Washing Effect on Ash Content

Throughout the project, samples were water washed as needed, and a cycle of freshly washed samples coming in, and previously washed samples being spend was developed. For each washing, sub-samples of mass were taken and processed by thermogravimetric analysis. The base feedstock, using 5 replications sampled at random, produced a mean ash content of 4.46% with a standard deviation of .31. In contrast, the water washed group spanned 8 sub-samples and produced a mean ash content of 2.80%, and a standard deviation of .45. This reduction is consistent with preliminary data obtained, and suggests that linear scale-up was successful. Table B.1 shows water washing to be significant at the 1% level for the reduction of ash content in the feedstock.

Table 4.4: Mineral analysis of pyrolysis feedstocks

Mineral Analysis (by wet chemistry)	Elephant Grass	WW	T250	T275
Ash % (from TGA)	4.46	2.80	2.74	4.49
Sodium (ppm)	118	<50	<50	<50
Potassium (%)	1.58	0.27	0.36	0.33
Magnesium (%)	0.15	0.11	0.13	0.13
Calcium (%)	0.22	0.21	0.30	0.30
Manganese (ppm)	40	38	46	46
Iron (ppm)	64	47	46	53
Copper (ppm)	<5	<5	<5	<5
Zinc (ppm)	52	30	34	34
Aluminum (ppm)	57	42	36	42
Phosphorus (%)	0.13	0.04	0.04	0.04
Sulfur (%)	0.04	0.01	0.02	0.02

Table 4.4 shows a qualitative mineral analysis of the elephant grass feedstocks. Of particular note, the alkali metals Sodium and Potassium showed a sharp decrease after water washing. These effects were less noticeable for the alkaline earth metals, however other select metals, such as Zinc, showed a marked decrease.

4.2 Grinding Energy Consumption

Table 4.5 shows the mean specific net energy and mean kWh/tonne for grinding of the biomass feedstocks. These data are consistent with expectations from the literature, and, due to lack of ultimate analysis, serve as a crude indication for increasing levels of treatment. These values are for the reduction of chops, previously hammer milled through a 1/2" screen, hammer milled through a 1/16" screen.

Additionally, Table 4.6 shows the particle size distribution for the ground feedstocks. The 1/16" screen provided a much smaller particle size than desired, with most of the mass being 315 µm or less. In Table 4.3 it is shown that torrefaction increased the bulk density after grinding.

Table 4.5: Grinding Energy Consumption Data

	Average kWh/tonne
Energy Cane Control	34.13 (3.63)
Elephant Grass Control	44.21 (2.76)
Elephant Grass WaterWashed	45.01 (9.82)
Elephant Grass Torrefied 250C	14.96 (0.761)
Elephant Grass Torrefied 275C	9.24 (1.67)

Due to issues presented during the course the project, a shortage of the 1/2" feedstock occurred. To continue with the project, feedstock that had been hammer milled through a 1/8" screen was used to make up the needed mass to operate the fluid bed reactor. Tables 4.7 and 4.8 show the particle size distributions and bulk densities of the original material, the extra material starting from 1/8" screen size, and the final combined value. The 1/2" and 1/8" group were ground separately through a 1/16" screen, and combined in a 1:1 mass ratio. This combined group was used for ALL fast pyrolysis testing.

Figure 4.3 shows the distribution of the ground materials and the shift to sub-500 particles. This is clearly seen in Figure 4.4 where as much as 75% or more of each feedstock is at 315 µm or lower.

Table 4.6: Particle size distribution of all feedstocks, ground

Particle Size Distribution (% mass)	Energy Cane	Elephant Grass	WW	T250	T275
1.25 mm	2.20 (0.36)	3.67 (0.11)	0.34 (0.10)	0.23 (0.06)	0.19 (0.10)
850 µm	13.82 (1.98)	18.35 (1.21)	7.43 (0.52)	1.73 (0.09)	0.75 (0.18)
500 µm	11.43 (1.53)	9.20 (0.85)	7.84 (0.36)	2.59 (0.25)	2.54 (0.43)
315 µm	32.05 (0.48)	29.20 (0.53)	31.52 (0.76)	23.72 (3.22)	21.59 (1.76)
200 µm	18.00 (0.43)	18.39 (0.20)	23.42 (0.40)	27.58 (2.00)	32.07 (1.30)
<200 µm	22.05 (4.77)	20.67 (0.80)	28.90 (0.31)	44.00 (1.63)	42.50 (1.09)

Table 4.7: Particle size distribution, T725

Particle Size Distribution (% mass)	T275 1/2" Initial	T275 1/8" Initial	T275 Combined
1.25 mm	0.19 (0.10)	0.07 (0.08)	0.04 (0.13)
850 µm	0.75 (0.18)	0.38 (0.14)	0.80 (0.05)
500 µm	2.54 (0.43)	1.24 (0.10)	1.85 (0.13)
315 µm	21.59 (1.76)	21.05 (1.73)	26.00 (2.24)
200 µm	32.07 (1.30)	30.69 (1.84)	28.69 (1.73)
<200 µm	42.50 (1.09)	47.83 (0.89)	42.29 (1.38)

Table 4.8: Bulk Density, T275

Bulk Density (kg/m3)	T275 1/2" Initial	T275 1/8" Initial	T275 Combined
Chopped	90.60 (2.58)		
Ground	243.19 (4.33)	207.69 (5.31)	225.86 (1.23)

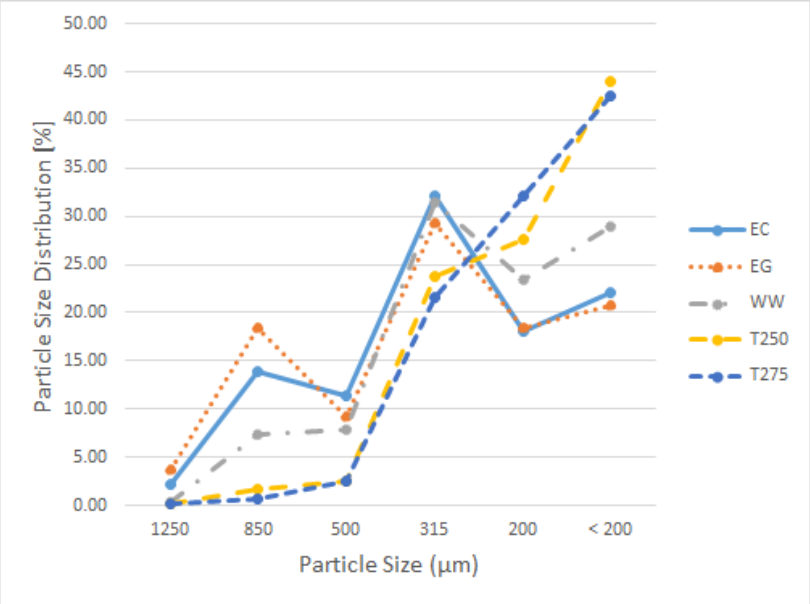

Figure 4.3: Particle size distribution of 1/16" feedstock

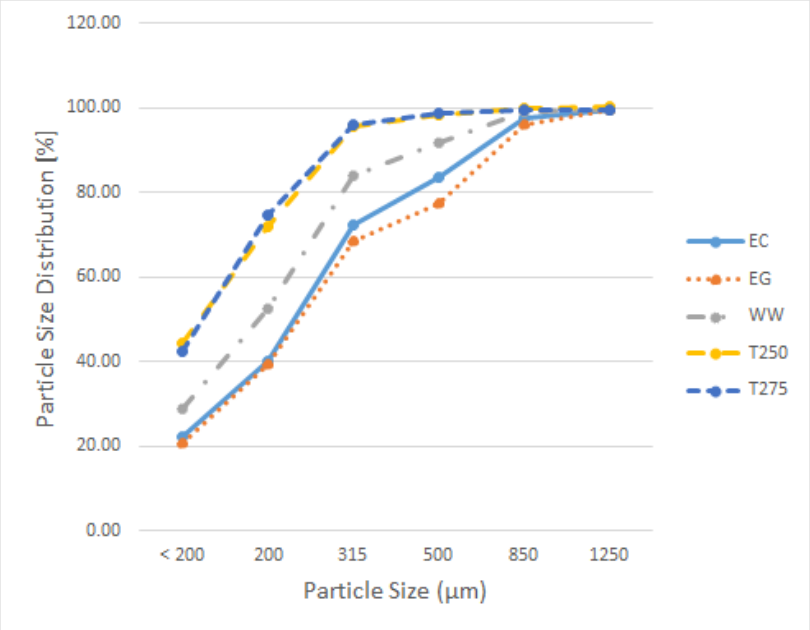

Figure 4.4: Cumulative passing graph for 1/2" feedstock

4.3 Fast Pyrolysis Product Yields

4.3.1 Effect of Water Washing

Each pyrolysis run was carried out in duplicate. ANOVA, shown in Table B.2, was done to compare the liquid yields of the control group to the water washed treatment. Water washing was found to have a significant impact at the 5% significance level, and the presence of the catalyst showed stronger impact being significant at the 1% level. Yields are displayed in Table 4.9; note that NCGs for all runs is the assumed mass difference. The liquid yield is notably lower than reported elsewhere in the literature, where numbers of 40-60% or higher can be found. This effect is seen throughout all runs, and is a result of the condensing system of the reactor. In particular, the lack of an electrostatic precipitator (ESP) diminishes the yield by an estimated 10-40%. The product collected is believed to be a representative condensate of the available product; as opposed to a fractional product whereby other fraction or fractions are not being condensed.

Table 4.9: Comparison of yields between control and water-washed groups, with and without catalyst

Yields %	Solid	Liquid	NCGs
Control	24.42 (3.66)	29.98 (1.48)	45.61 (5.13)
Control w/ Cat	19.19 (1.05)	26.63 (1.92)	54.19 (0.87)
WW	13.87 (0.11)	28.59 (0.93)	57.55 (0.93)
WW w/ Cat	21.54 (2.18)	22.82 (0.37)	55.65 (2.54)

The bio char produced was analyzed, with particular interest in the volatile content. Volatile content is used as a rough indicator of how effectively the system pyrolyzed the feedstock. The TGA method heats samples to 900°C during the volatile determination step, so there is expected to be some amount of higher volatile content available at such a temperature. With the mean value of volatile content, shown in Table 4.10, in the low 30 percentile range, it is concluded that a reasonable amount of pyrolytic activity is occurring

Table 4.10: Volatile and Fixed Carbon comparison of water wash experiment with and without catalyst

Proximate Analysis, Dry, Ash free (%)	Volatile	Fixed Carbon
Control	32.14 (1.84)	67.86 (1.84)
Control w/ Cat	40.74 (9.39)	59.26 (9.39)
WW	32.43 (0.94)	67.57 (0.94)
WW w/ Cat	61.91 (13.83)	38.09 (13.83)

based on similar literature projects such as [53]. For the catalytic runs, a higher volatile content is seen, with the water washed catalytic run having 60% volatile content remaining. This effect is common throughout the study and indicates that, while it may be catalytically active, red mud may not be suitable as bed material in the fluid bed reactor.

HPLC

HPLC analyses of the polar fraction obtained from pyrolysis runs showed high concentrations of four products: levoglucosan, formate, acetate, and hydroxyacectone. Other compounds were detected at low concentrations, e.g. 2 g/L or less (see Appendix D for full product distribution). Additionally, a higher than expected fraction of DCM dissolved into the polar fraction upon separation. It is believe the high concentration of other compounds than water allowed for this higher volume to exist. Calculations were done to adjust for the presence of DCM and revert concentrations to a DCM free value. Water washing, as well as catalyst presence, were both significant at the 1% level. Water washing worked to increase the levoglucosan production, while red mud catalyzed levoglucosan into other products, somewhat negating the effects of each other. Formate, acetate, and hydroxyacetone followed the same trend for significance and concentration. Table 4.11 shows the mean concentrations of these four products.

Table 4.11: HPLC concentrations for WW and Control

Mean Concentration, g/L	Levoglucosan	Formate	Acetate	Hydroxyacetone
Control	59.78 (11.73)	33.08 (19.64)	76.22 (15.13)	41.89 (8.27)
Control w/ Cat	13.13 (2.36)	11.01 (2.94)	45.45 (8.57)	23.10 (4.29)
WW	224.39 (31.13)	96.52 (54.24)	129.78 (23.89)	59.56 (14.42)
WW w/ Cat	61.38 (10.77)	44.99 (7.76)	93.06 (15.32)	47.42 (7.71)

4.3.2 Effect of Torrefaction

Yields for torrefaction and subsequent pyrolysis are shown in Table 4.12. More replications were desired to acquire a more precise value for the T275 runs; however, the necessary mass to complete that run was consumed in the catalytic runs. Table B.7 find that both catalyst and torrefaction have statistical significance at the 1% level for liquid yields.

Table 4.12: Torrefaction and Catalytic Pyrolysis yields

Yield %	Solid	Liquid	NCGs
Torrefaction			
250	81.08 (4.12)		
275	71.50 (1.23)		
Pyrolysis			
WW	13.87 (0.11)	28.59 (0.93)	57.55 (1.04)
WW w/ Cat	21.54 (2.18)	22.82 (0.37)	55.65 (2.54)
T250	28.68 (0.25)	23.58 (1.10)	47.75 (1.35)
T250 w/ Cat	18.07 (4.82)	13.46 (4.65)	68.48 (9.48)
T275	37.79 (10.95)	19.62 (0.07)	42.58 (10.88)
T275 w/ Cat	36.34 (0.03)	15.92 (1.36)	47.74 (1.39)

Table 4.13 shows the comparison of dry, ash free volatiles and fixed carbon. As previously discussed, catalytic runs do not perform as well as non-catalytic runs in terms of mean volatile content reduction. While the number of replications is low, this data serves as a preliminary reference suggesting that red mud, as treated for this study, is not as effective, as a heat transfer medium, as sand.

Table 4.13: Dry, ash free comparison of WW, T250, T275 volatile content

Proximate Analysis, Dry, Ash free (%)	Volatile	Fixed Carbon
WW	32.43 (0.94)	67.57 (0.94)
WW w/ Cat	61.91 (13.83)	38.09 (13.83)
T250	28.68 (0.26)	71.32 (0.26)
T250 w/ Cat	37.20 (4.76)	62.80 (4.76)
T275	27.62 (0.50)	72.38 (0.50)
T275 w/ Cat	41.20 (5.20)	58.80 (5.20)

Table 4.14: HPLC Concentrations for WW, T250, and T275

Mean Concentration, g/L	Levoglucosan	Formate	Acetate	Hydroxyacetone
WW	224.39 (31.13)	96.52 (54.24)	129.78 (23.89)	59.56 (14.42)
WW w/ Cat	61.38 (10.77)	44.99 (7.76)	93.06 (15.32)	47.42 (7.71)
T250	152.00 (28.24)	62.45 (42.27)	95.66 (17.09)	47.57 (7.41)
T250 w/ Cat	49.63 (21.64)	34.42 (13.88)	59.37 (18.78)	31.17 (7.97)
T275	171.44 (40.14)	80.54 (35.98)	74.96 (16.12)	35.52 (10.25)
T275 w/ Cat	45.80 (27.24)	31.91 (12.81)	44.23 (17.22)	22.04 (8.17)

HPLC

ANOVA for each of the 4 previously discussed compounds was completed. The catalyst showed strong effect for levoglucosan concentration, statistically significant at the 1% level. However, that was the only compound which it showed significance for. Torrefaction treatment (again, water washing is the 'control' for these tables) was significant for levoglucosan at the 5% level, and significant at the 1% level for formate, acetate, and hydroxyacetone. Additionally, there was a strong (1% significance) interaction effect for these three compounds as well. The interaction effect was not significant for levoglucosan. Means and standard deviations are reported in Table 4.14.

Coke Formation

Table 4.15 shows mean coke values obtained from the project. The entire sand bed was burned for coke value and the mean value of pyrolysis replications is shown. Duplicate samples of catalyst were burned for each pyrolysis replication, and the mean of these four values are displayed in place. Figure 4.5 shows the limitation of the data to identify effects on

Table 4.15: Mean Coke Formation

Group	Mean Coke %
EG w/ Cat	23.00 (2.91)
WW	8.41 (0.57)
WW w/ Cat	20.06 (2.61)
T250	3.61 (0.81)
T250 w/ Cat	23.02 (3.93)
T275	4.46 (2.98)
T275 w/ Cat	20.78 (3.23)

coke formation. More replications are required to successfully determine the exact outcome of treatments on coke formation. Torrefaction reduced coke formation for the control groups, but mean values increased in the presence of catalyst. Additionally, residual biomass present in the bed post-run skew the data. A study that is more tightly controlled for mass flow into and out of the bed will be required to determine these effects. Further discussion related to this can be found in Appendix A.

4.4 Further HPLC Discussion

It is worth noting that for the water washed trials, over 200 g/L of levoglucosan was produced. One possible explanation for the data is that red mud preferentially catalyzes levoglucosan, and this high load of substrate deactivates the catalyst for other compounds. Additionally, while water washing removes some of the alkali metal content from the feedstock, some alkali metal is being reintroduced to the system by the catalyst composition. This could

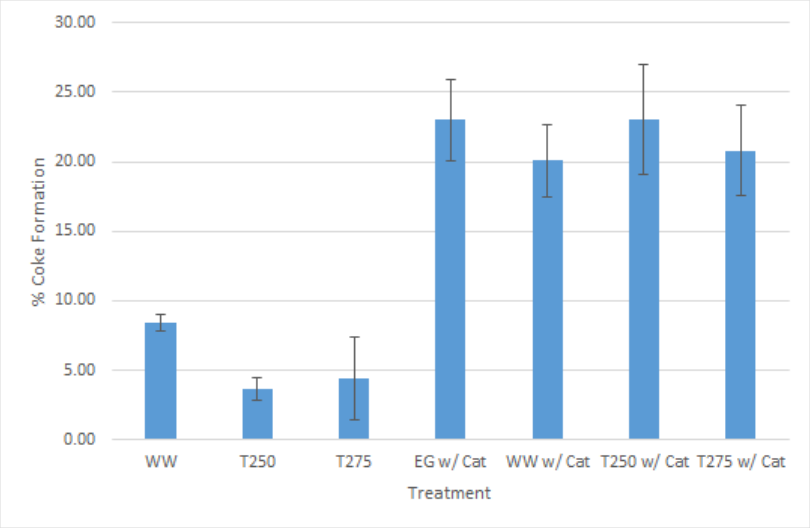

Figure 4.5: Comparison of coke formation

lead to a confounding effect within the study. With regard to torrefaction, the T250 group would see degredation of hemicellulose, thus decreasing production of formate, acetate in the pyrolysis product. The higher group would see the degredation of cellulose, leading to a decrease in available levoglucosan and hydroxyacetaldehyde. This would manifest as lower concentrations of levoglucosan, formate, acetate, and hydroxyacetone. Further, reduction of total alkali metal was expected to increase levoglucosan while decreasing formate and acetate production. The data collected, combined with data from the previous section, suggest that levoglucosan production is more sensitive to the presence of alkali metals than hydroxyacetaldehyde. Torrefaction actively works to counter the production of all 3 of these species, and as such serves as a poor treatment option when combined with water washing for the purpose of this study.

Figure 4.6 show the changes in mean levoglucosan concentration between all groups. In particular, the high water wash value is seen, with its effect so much that it carries into the torrefaction groups. All catalyst runs show a 3-4 fold reduction in levoglucosan concentration.

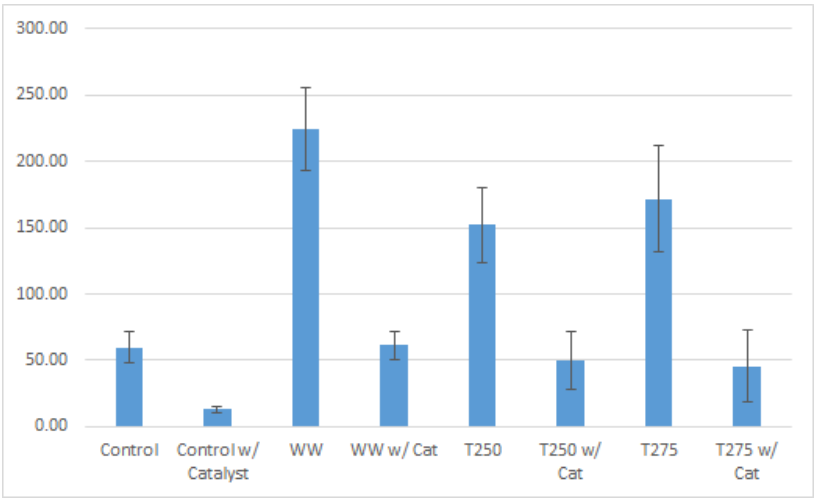

Figure 4.6: Mean levoglucosan concentration across all groups

In Figure 4.7, the same trend for means can be seen; however, the error bars present a much larger range here. Interestingly, the catalyst runs seem to be more consistent, averaging lower standard deviations than the non-catalytic runs. This data shows a need for more replications with the reactor.

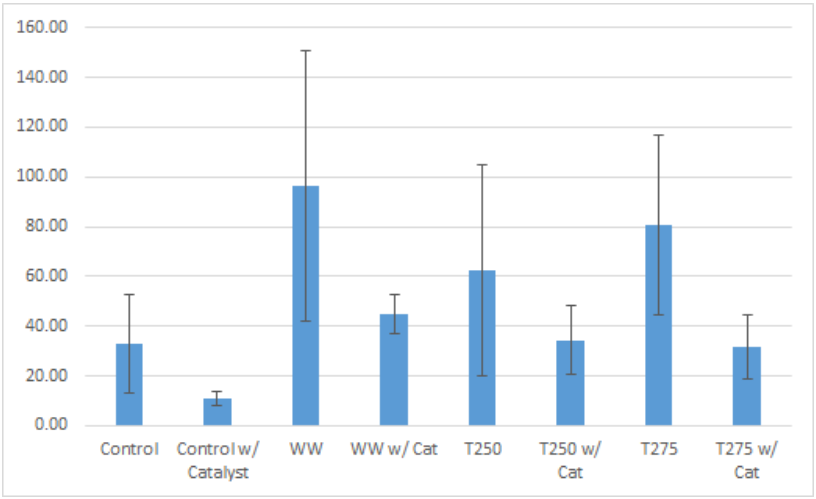

Figure 4.7: Mean formate concentration across all groups

Acetate and hydroxyacetone have similar distribution patterns for all runs, with hy-

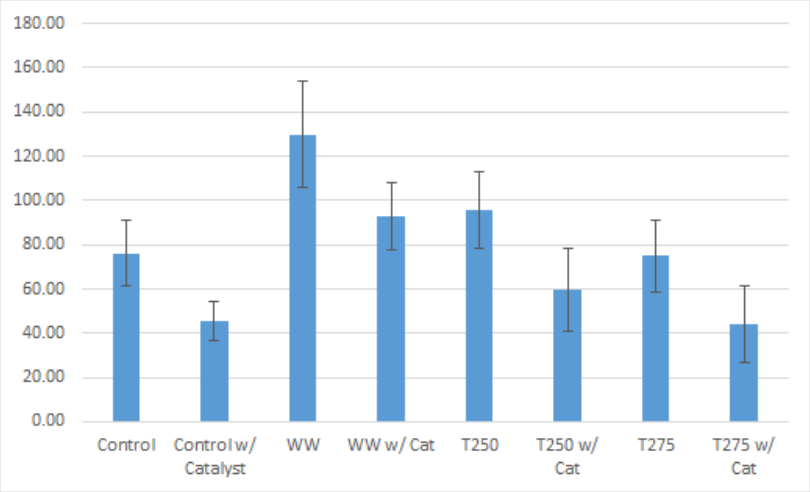

Figure 4.8: Mean acetate concentration across all groups

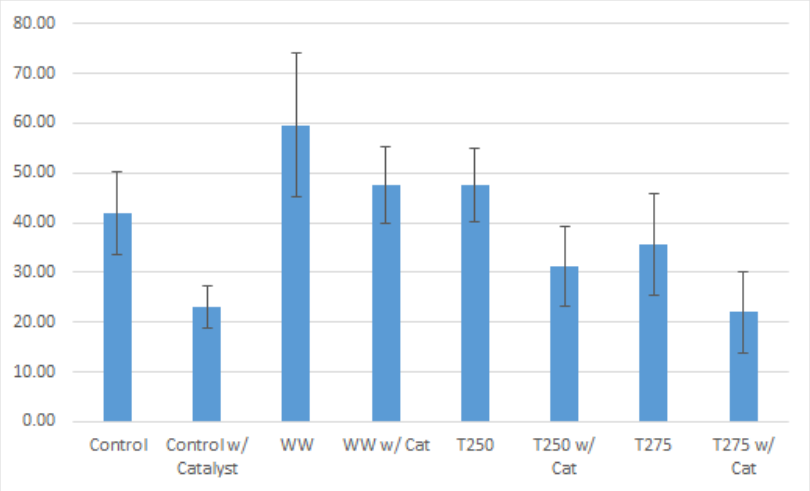

Figure 4.9: Mean hydroxyacetone concentration across all groups

droxyacetone typically being half of the concentration of acetone. These results follow the mechanisms discussed in [62]

4.5 Liquid Yield Distribution

As part of the mass balance process, the individual masses for each component involved in liquid collect was obtained. These data are present in Table 4.16, where 'water bath collectors' is the final three canisters combined. Mass values have been normalized to a percent of available liquid yield. Of particular note is the shift in mass distribution, depicted in Figure 4.10, to the water bath collectors on catalytic runs. This data is somewhat empirical, but the mass of the condenser is very thick and non-fluid, the mass in canister three looks and flows like motor oil, while the water bath collector fraction appears very aqueous in nature. Using these data as indicators, catalytic runs preferentially shift liquid products to water-soluble components. Water washing had a weaker effect, slightly decreasing mean water bath collector mass; however, torrefaction parameters increased water bath collector mass to a higher degree than even the unwashed feedstock.

Table 4.16: Liquid Yield Distribution

Liquid Yield %	Condenser	Canister 3	Water Bath Collectors
Control	23.92 (0.91)	49.12 (1.24)	26.96 (0.33)
Control w/ Cat	19.45 (5.59)	37.65 (5.44)	42.91 (11.03)
WW	24.33 (2.26)	53.72 (4.38)	21.96 (2.12)
WW w/ Cat	27.88 (4.08)	25.03 (6.39)	47.09 (2.31)
T250	29.23 (4.06)	21.53 (8.12)	39.23 (4.06)
T250 w/ Cat	26.45 (2.06)	24.13 (1.23)	49.42 (0.82)
T275	41.18 (3.25)	21.68 (3.16)	37.14 (6.40)
T275 w/ Cat	30.60 (5.21)	10.49 (9.40)	58.90 (14.61)

4.6 Liquid HHV

Higher heating values of the liquid samples, excluding the condenser coil components (hereafter simply 'condenser' fraction), have been collected in replicate for each trial. However, due to the moisture content within the samples, it was necessary to use a combustion aid (in

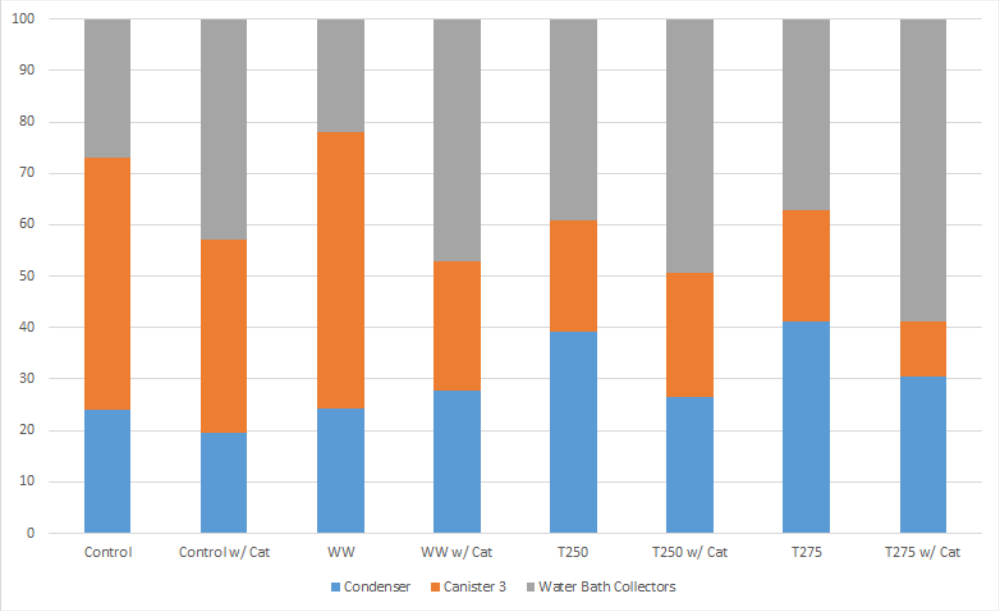

Figure 4.10: Breakdown of Liquid Yield, Normalized

this case, olive oil) to retrieve data. These values are presented in Table 4.17. It is believed that these values are reasonably accurate, and the remaining HHV from the expected value is locked in the condenser fraction.

4.7 Brief Analysis of Energy Cane Data

Energy cane was processed at the start of the study as a test material to establish operating parameters and procedures. Physical properties are presented alongside Napier grass at the beginning of the chapter as an added comparison. Table 4.18 shows the mass balance results from fast pyrolysis of energy cane. While statistical data is unavailable for these runs, the liquid yields fit the expectation set by the Napier grass runs.

Table 4.19 shows concentrations for the energy cane product. As a preliminary test, this process showed strong catalytic activity and promising results.

Table 4.17: Higher Heating Values by Rep

	Mean HHV, MJ/kg
Energy Cane Sand	6.858 (0.100)
Energy Cane RMC	2.937 (0.064)
Elephant Grass Control Sand Rep 1	4.981 (0.186)
Elephant Grass Control Sand Rep 2	5.642 (0.186)
Elephant Grass Control RMC Rep 1	2.574 (0.071)
Elephant Grass Control RMC Rep 2	1.559 (0.460)
Elephant Grass WaterWashed Sand Rep 1	12.993 (0.196)
Elephant Grass WaterWashed Sand Rep 2	12.964 (0.215)
Elephant Grass WaterWashed RMC Rep 1	8.593 (0.613)
Elephant Grass WaterWashed RMC Rep 2	10.893 (1.685)
Elephant Grass Torrefied 250C Sand Rep 1	7.974 (0.254)
Elephant Grass Torrefied 250C Sand Rep 2	10.426 (0.750)
Elephant Grass Torrefied 250C RMC Rep 1	10.877 (4.021)
Elephant Grass Torrefied 250C RMC Rep 2	7.591 (2.091)
Elephant Grass Torrefied 275C Sand Rep 1	10.823 (0.693)
Elephant Grass Torrefied 275C Sand Rep 2	9.480 (0.119)
Elephant Grass Torrefied 275C RMC Rep 1	1.668 (0.251)
Elephant Grass Torrefied 275C RMC Rep 2	7.078 (0.810)

Table 4.18: Fast pyrolysis yields for Energy Cane

Yield %	Solid	Liquid	NCGs
Control	19.51	31.17	49.32
Catalyst	21.54	22.05	56.41

Table 4.19: HPLC of Energy Cane Product

	Levoglucosan	Formate	Acetate	Hydroxyacetone
Control	63.40 (2.55)	45.02 (1.87)	68.33 (3.08)	29.75 (1.35)
Catalyst	0.00 (0.00)	14.70 (0.07)	44.13 (0.37)	18.84 (0.44)

4.7.1 GC-MS

Tables 4.20 and 4.21 show the product distribution for the energy cane control run. The TAM fraction has a higher showing for hydrocarbons, alcohols, phenols, acids, and benzene, while DCM had higher values of ketones, esters, and aldehydes. The expected results of catalytic runs would be a decrease in acidic compounds with a higher value of hydrocarbons, phenols, and ketones. Torrefaction is expected to harshly reduce acid production. Based on HPLC data obtained, wasterwashing is expected to increase acidic compounds. Tables C.1 and C.2 show retention times by compound.

Table 4.20: Product composition of DCM fraction

Compound Type	Area Percent
alkene	6.5
alkane	0.0
alkyne	0.3
HC	6.8
Alcohol	7.8
Ketone	31.1
Ester	4.4
Phenol	6.2
Acids	2.9
Furan	0.0
Aldehyde	0.0
benzene	6.2
toluene	0.0
ethylbenzene	0.0
p-xylene	0.0
m-xylene	0.0
BTEX	6.2
linoleic acid	0.0
oleic acid	0.0
palmitic acid	0.0
FFA	0.0
N-containing	0.1
Methylene chloride	N/A
1-hexanol	0.0
heptane	N/A

Table 4.21: Product composition of TAM fraction

Compound Type	Area Percent
alkene	7.5
alkane	0.3
alkyne	0.0
HC	7.8
Alcohol	8.4
Ketone	11.2
Ester	0.3
Phenol	8.4
Acids	7.6
Furan	0.0
Aldehyde	2.3
benzene	8.4
toluene	0.0
ethylbenzene	0.4
p-xylene	0.0
m-xylene	1.0
BTEX	9.7
linoleic acid	0.0
oleic acid	0.0
palmitic acid	1.4
FFA	1.4
N-containing	7.9
Methylene chloride	N/A
1-hexanol	0.0
heptane	N/A

Chapter 5

Conclusions and Recommendations

5.1 Summary Conclusions

Physical Properties and Grinding

Water washing is an effect method for leeching alkali metals from biomass. A more refined procedure may be able to achieve even lower ash and alkali content. Torrefaction is effective at carbonization of feedstock, but product quality as analyzed by HPLC suggest this may be counter-productive on water washed materials. Grinding energy was greatly reduced for torrefied groups, which may prove an important factor for future studies seeking to balance feedstock parameters with transport logistics. Hammer milling through 1/16" screen overshot the target size of 1 mm and future studies may wish to investigate using 1/8" or a 'multi-pass' grinding with larger screen sizes.

Bio-oil Yield

Yields for all processes were 30% or less. While the product collected is believed to be representative, true yield potentials are skewed by condensation limits. With the data available, reductions in liquid yield are quantitatively shown for catalyst presence and torrefaction

severity. Future studies may seek to quantify an optimal procedure balancing total yield with yield quality based on a full array of data.

Char Yield

Biochar produced was more consistent between runs than liquid gas. Catalyst runs produced a char with higher volatile content, indicating that full pyrolysis may not be achieved. This is based on volatile matter being the fraction released during pyrolysis, forming liquid products, NCGs, and water. As such, higher volatile matter indicates more product is remaining in the char product. Recirculation of the char through the bed, as with a circulating fluid bed, may provide a more complete pyrolysis of the feedstock, improving liquid yields for catalytic runs. This effect may be confounding the liquid yield of catalytic runs, masking the true potential value.

Bio-oil Quality

Ash reduction via water washing increased yields of levoglucosan, formate, acetate, and hydroxyacetone. Additionally, lower solid yield was obtain from the fast pyrolysis of the water washed sample. Torrefaction worked in opposite, decreasing yields of the aforementioned compounds, as well as total liquid yield, with severity increasing this effect. Red mud is effective at catalyzing the target compounds, further reversing the effect of water washing.

Liquid Yield Distribution

For all catalytic runs, though less total liquid may be produced, more of that liquid product is diverted to the water-soluble fraction. Water washing produced a mildly decreased water-soluble fraction, and torrefaction, which also decreased available liquid yields, shifted products to water-soluble compounds.

5.2 Recommendations

Ash reduction via water washing proved effective; however there may be room for improvement. Future studies may consider refining the water washing protocol, or shifting to an acid washing process. Water washing in tandem with torrefaction, or red mud as prepared here, appears to be a poor match. The treatments are opposite and confounding. Torrefaction of base, non-washed feedstocks should be investigated to test it's effects with red mud. It may, potentially, be worthwhile with a lower ash product to try torrefaction again.

Red mud ultimately worked as a catalyst, but did not perform as was desired by the volatile content metric. It is the opinion of the author that future works using red mud as a catalyst either, devote studies to reforming the catalyst into a more durable particle for fluidzation, or use red mud in a secondary bed as an in-line vapor stream upgrade, while using sand or some other well establish heat transfer media. Further rationale and a deeper explanation of key reactor principles can be located in Appendix A.

Bibliography

[1] Mark Downing, Laurence M Eaton, Robin Lambert Graham, Matthew H Langholtz, Robert D Perlack, Anthony F Turhollow Jr, Bryce Stokes, and Craig C Brandt. Us billion-ton update: Biomass supply for a bioenergy and bioproducts industry. Technical report, Oak Ridge National Laboratory (ORNL), 2011.

[2] Bruce S Dien, Hans-Joachim G Jung, Kenneth P Vogel, Michael D Casler, JoAnn FS Lamb, Loren Iten, Robert B Mitchell, and Gautum Sarath. Chemical composition and response to dilute-acid pretreatment and enzymatic saccharification of alfalfa, reed canarygrass, and switchgrass. *Biomass and Bioenergy*, 30(10):880–891, 2006.

[3] Peter McKendry. Energy production from biomass (part 1): overview of biomass. *Bioresource technology*, 83(1):37–46, 2002.

[4] Charles A Mullen, Akwasi A Boateng, et al. Chemical composition of bio-oils produced by fast pyrolysis of two energy crops. *Energy Fuels*, 22(3):2104–2109, 2008.

[5] Russell W Jessup. Development and status of dedicated energy crops in the united states. *In Vitro Cellular & Developmental Biology-Plant*, 45(3):282–290, 2009.

[6] Misook Kim and Donal F Day. Composition of sugar cane, energy cane, and sweet sorghum suitable for ethanol production at louisiana sugar mills. *Journal of industrial microbiology & biotechnology*, 38(7):803–807, 2011.

[7] Food and agriculture organization of the united nations. http://faostat.fao.org/site/567/DesktopDefault.aspx?PageID=567. Accessed: 2016-02-19.

[8] Sizuo Matsuoka, Anthony J Kennedy, Eder Gustavo D dos Santos, André L Tomazela, and Luis Claudio S Rubio. Energy cane: its concept, development, characteristics, and prospects. *Advances in Botany*, 2014, 2014.

[9] D Wang, JA Poss, TJ Donovan, MC Shannon, and SM Lesch. Biophysical properties and biomass production of elephant grass under saline conditions. *Journal of Arid Environments*, 52(4):447–456, 2002.

[10] Rafael Fiusa de Morais, Bruno Juscelino de Souza, José Marcos Leite, Luis Henrique de Barros Soares, Bruno José Rodrigues Alves, Robert Michael Boddey, and Segundo Urquiaga. Elephant grass genotypes for bioenergy production by direct biomass combustion. *Pesquisa Agropecuária Brasileira*, 44(2):133–140, 2009.

[11] Vladimir Strezov, Tim J Evans, and Chris Hayman. Thermal conversion of elephant grass (pennisetum purpureum schum) to bio-gas, bio-oil and charcoal. *Bioresource technology*, 99(17):8394–8399, 2008.

[12] Rahman Saidur, EA Abdelaziz, Ayhan Demirbas, MS Hossain, and S Mekhilef. A review on biomass as a fuel for boilers. *Renewable and Sustainable Energy Reviews*, 15(5):2262–2289, 2011.

[13] Jiuan Jing Chew and Veena Doshi. Recent advances in biomass pretreatment–torrefaction fundamentals and technology. *Renewable and Sustainable Energy Reviews*, 15(8):4212–4222, 2011.

[14] AV Bridgwater, D Meier, and D Radlein. An overview of fast pyrolysis of biomass. *Organic Geochemistry*, 30(12):1479–1493, 1999.

[15] Stefan Czernik and AV Bridgwater. Overview of applications of biomass fast pyrolysis oil. *Energy & Fuels*, 18(2):590–598, 2004.

[16] Anthony V Bridgwater. Review of fast pyrolysis of biomass and product upgrading. *Biomass and bioenergy*, 38:68–94, 2012.

[17] AV Bridgwater. Production of high grade fuels and chemicals from catalytic pyrolysis of biomass. *Catalysis today*, 29(1):285–295, 1996.

[18] Tristan R Brown, Rajeeva Thilakaratne, Robert C Brown, and Guiping Hu. Techno-economic analysis of biomass to transportation fuels and electricity via fast pyrolysis and hydroprocessing. *Fuel*, 106:463–469, 2013.

[19] Mark M Wright, Daren E Daugaard, Justinus A Satrio, and Robert C Brown. Techno-economic analysis of biomass fast pyrolysis to transportation fuels. *Fuel*, 89:S2–S10, 2010.

[20] Feroz Kabir Kazi, Joshua A Fortman, Robert P Anex, David D Hsu, Andy Aden, Abhijit Dutta, and Geetha Kothandaraman. Techno-economic comparison of process technologies for biochemical ethanol production from corn stover. *Fuel*, 89:S20–S28, 2010.

[21] Ryan M Swanson, Alexandru Platon, Justinus A Satrio, and Robert C Brown. Techno-economic analysis of biomass-to-liquids production based on gasification. *Fuel*, 89:S11–S19, 2010.

[22] Qi Zhang, Jie Chang, Tiejun Wang, and Ying Xu. Review of biomass pyrolysis oil properties and upgrading research. *Energy conversion and management*, 48(1):87–92, 2007.

[23] Peter Mølgaard Mortensen, J-D Grunwaldt, Peter Arendt Jensen, KG Knudsen, and Anker Degn Jensen. A review of catalytic upgrading of bio-oil to engine fuels. *Applied Catalysis A: General*, 407(1):1–19, 2011.

[24] Dinesh Mohan, Charles U Pittman, and Philip H Steele. Pyrolysis of wood/biomass for bio-oil: a critical review. *Energy & Fuels*, 20(3):848–889, 2006.

[25] Snigdha Sushil and Vidya S Batra. Catalytic applications of red mud, an aluminium industry waste: A review. *Applied Catalysis B: Environmental*, 81(1):64–77, 2008.

[26] Jyotsnamayee Pradhan, Jasobanta Das, Surendranath Das, and Ravindra Singh Thakur. Adsorption of phosphate from aqueous solution using activated red mud. *Journal of colloid and interface science*, 204(1):169–172, 1998.

[27] A López, I De Marco, BM Caballero, MF Laresgoiti, A Adrados, and A Aranzabal. Catalytic pyrolysis of plastic wastes with two different types of catalysts: Zsm-5 zeolite and red mud. *Applied Catalysis B: Environmental*, 104(3):211–219, 2011.

[28] Elham Karimi, Cedric Briens, Franco Berruti, Sina Moloodi, Tommy Tzanetakis, Murray J Thomson, and Marcel Schlaf. Red mud as a catalyst for the upgrading of hemp-seed pyrolysis bio-oil. *Energy & Fuels*, 24(12):6586–6600, 2010.

[29] Bhuvanesh K Yathavan and FA Agblevor. Catalytic pyrolysis of pinyon–juniper using red mud and hzsm-5. *Energy & Fuels*, 27(11):6858–6865, 2013.

[30] Jiajia Meng, Junyeong Park, David Tilotta, and Sunkyu Park. The effect of torrefaction on the chemistry of fast-pyrolysis bio-oil. *Bioresource technology*, 111:439–446, 2012.

[31] Janewit Wannapeera, Bundit Fungtammasan, and Nakorn Worasuwannarak. Effects of temperature and holding time during torrefaction on the pyrolysis behaviors of woody biomass. *Journal of Analytical and Applied Pyrolysis*, 92(1):99–105, 2011.

[32] Vaishnavi Srinivasan, Sushil Adhikari, Shyamsundar Ayalur Chattanathan, and Sunkyu Park. Catalytic pyrolysis of torrefied biomass for hydrocarbons production. *Energy & Fuels*, 26(12):7347–7353, 2012.

[33] Anqing Zheng, Zengli Zhao, Zhen Huang, Kun Zhao, Guoqiang Wei, Xiaobo Wang, Fang He, and Haibin Li. Catalytic fast pyrolysis of biomass pretreated by torrefaction with varying severity. *Energy & Fuels*, 28(9):5804–5811, 2014.

[34] CCRC. Plant cell wall basics. [Online; accessed 20-August-2015].

[35] Bo Madsen and E Kristofer Gamstedt. Wood versus plant fibers: similarities and differences in composite applications. *Advances in Materials Science and Engineering*, 2013, 2013.

[36] Tansy Wigley, Alex CK Yip, and Shusheng Pang. The use of demineralisation and torrefaction to improve the properties of biomass intended as a feedstock for fast pyrolysis. *Journal of Analytical and Applied Pyrolysis*, 113:296–306, 2015.

[37] Tansy Wigley, Alex CK Yip, and Shusheng Pang. Pretreating biomass via demineralisation and torrefaction to improve the quality of crude pyrolysis oil. *Energy*, 109:481–494, 2016.

[38] Daniel J Nowakowski, Jenny M Jones, Rik MD Brydson, and Andrew B Ross. Potassium catalysis in the pyrolysis behaviour of short rotation willow coppice. *Fuel*, 86(15):2389–2402, 2007.

[39] Donald S Scott, Lachlan Paterson, Jan Piskorz, and Desmond Radlein. Pretreatment of poplar wood for fast pyrolysis: rate of cation removal. *Journal of Analytical and Applied Pyrolysis*, 57(2):169–176, 2001.

[40] R Fahmi, Anthony V Bridgwater, I Donnison, Nicola Yates, and JM Jones. The effect of lignin and inorganic species in biomass on pyrolysis oil yields, quality and stability. *Fuel*, 87(7):1230–1240, 2008.

[41] Manunya Phanphanich and Sudhagar Mani. Impact of torrefaction on the grindability and fuel characteristics of forest biomass. *Bioresource technology*, 102(2):1246–1253, 2011.

[42] Wei Yan, Tapas C Acharjee, Charles J Coronella, and Victor R Vásquez. Thermal pretreatment of lignocellulosic biomass. *Environmental Progress & Sustainable Energy*, 28(3):435–440, 2009.

[43] Mark J Prins, Krzysztof J Ptasinski, and Frans JJG Janssen. Torrefaction of wood: Part 2. analysis of products. *Journal of analytical and applied pyrolysis*, 77(1):35–40, 2006.

[44] Wei Yan, Jason T Hastings, Tapas C Acharjee, Charles J Coronella, and Victor R Vasquez. Mass and energy balances of wet torrefaction of lignocellulosic biomass. *Energy & Fuels*, 24(9):4738–4742, 2010.

[45] Shoujie Ren, Hanwu Lei, Lu Wang, Quan Bu, Shulin Chen, Joan Wu, James Julson, and Roger Ruan. The effects of torrefaction on compositions of bio-oil and syngas from biomass pyrolysis by microwave heating. *Bioresource technology*, 135:659–664, 2013.

[46] Dmitri A Bulushev and Julian RH Ross. Catalysis for conversion of biomass to fuels via pyrolysis and gasification: a review. *Catalysis Today*, 171(1):1–13, 2011.

[47] Richard French and Stefan Czernik. Catalytic pyrolysis of biomass for biofuels production. *Fuel Processing Technology*, 91(1):25–32, 2010.

[48] Qiang Lu, Zhi-Fei Zhang, Chang-Qing Dong, and Xi-Feng Zhu. Catalytic upgrading of biomass fast pyrolysis vapors with nano metal oxides: an analytical py-gc/ms study. *Energies*, 3(11):1805–1820, 2010.

[49] Foster A Agblevor, Douglas C Elliott, Daniel M Santosa, Mariefel V Olarte, Sarah D Burton, Marie Swita, Sedat H Beis, Kyle Christian, and Brandon Sargent. Red mud catalytic pyrolysis of pinyon juniper and single-stage hydrotreatment of oils. *Energy & Fuels*, 2016.

[50] Fast Pyrolysis. Process design and economics for the conversion of lignocellulosic biomass to hydrocarbon fuels. 2013.

[51] AV Bridgwater. Renewable fuels and chemicals by thermal processing of biomass. *Chemical Engineering Journal*, 91(2):87–102, 2003.

[52] AV Bridgwater and GVC Peacocke. Fast pyrolysis processes for biomass. *Renewable and sustainable energy reviews*, 4(1):1–73, 2000.

[53] Akwasi A Boateng, Daren E Daugaard, Neil M Goldberg, and Kevin B Hicks. Bench-scale fluidized-bed pyrolysis of switchgrass for bio-oil production. *Industrial & Engineering Chemistry Research*, 46(7):1891–1897, 2007.

[54] RW Nachenius, Frederik Ronsse, RH Venderbosch, and Wolter Prins. Biomass pyrolysis. *Chemical engineering for renewables conversion*, 42:75–139, 2013.

[55] T Melkior, S Jacob, G Gerbaud, S Hediger, L Le Pape, L Bonnefois, and M Bardet. Nmr analysis of the transformation of wood constituents by torrefaction. *Fuel*, 92(1):271–280, 2012.

[56] Colomba Di Blasi, Antonio Galgano, and Carmen Branca. Influences of the chemical state of alkaline compounds and the nature of alkali metal on wood pyrolysis. *Industrial & Engineering Chemistry Research*, 48(7):3359–3369, 2009.

[57] José M Encinar, Fernando J Beltrán, Antonio Ramiro, and Juan F González. Catalyzed pyrolysis of grape and olive bagasse. influence of catalyst type and chemical treatment. *Industrial & engineering chemistry research*, 36(10):4176–4183, 1997.

[58] Roger N Hilten, Richard A Speir, James R Kastner, Sudhagar Mani, and KC Das. Effect of torrefaction on bio-oil upgrading over hzsm-5. part 1: Product yield, product quality, and catalyst effectiveness for benzene, toluene, ethylbenzene, and xylene production. *Energy & Fuels*, 27(2):830–843, 2013.

[59] AA Boateng and CA Mullen. Fast pyrolysis of biomass thermally pretreated by torrefaction. *Journal of Analytical and Applied Pyrolysis*, 100:95–102, 2013.

[60] Exxon Mobil. The outlook for energy: A view to 2040. *Exxon Mobil*, 2014.

[61] Fred Sissine. Energy independence and security act of 2007: a summary of major provisions. DTIC Document, 2007.

[62] DSAG Radlein, J Piskorz, and DS Scott. Fast pyrolysis of natural polysaccharides as a potential industrial process. *Journal of Analytical and Applied Pyrolysis*, 19:41–63, 1991.

[63] Shuangning Xiu and Abolghasem Shahbazi. Bio-oil production and upgrading research: A review. *Renewable and Sustainable Energy Reviews*, 16(7):4406–4414, 2012.

[64] S Şensöz, D Angın, and S Yorgun. Influence of particle size on the pyrolysis of rapeseed (brassica napus l.): fuel properties of bio-oil. *Biomass and Bioenergy*, 19(4):271–279, 2000.

[65] R Vance Morey, Nalladurai Kaliyan, Douglas G Tiffany, and David R Schmidt. A corn stover supply logistics system. *Applied Engineering in Agriculture*, 26(3):455–461, 2010.

[66] Serdar Yaman. Pyrolysis of biomass to produce fuels and chemical feedstocks. *Energy conversion and management*, 45(5):651–671, 2004.

[67] Dorde Medic, M Darr, A Shah, B Potter, and J Zimmerman. Effects of torrefaction process parameters on biomass feedstock upgrading. *Fuel*, 91(1):147–154, 2012.

[68] Chris Somerville, Heather Youngs, Caroline Taylor, Sarah C Davis, Stephen P Long, et al. Feedstocks for lignocellulosic biofuels. *Science(Washington)*, 329(5993):790–792, 2010.

[69] Sudhagar Mani, Lope G Tabil, and Shahab Sokhansanj. Grinding performance and physical properties of wheat and barley straws, corn stover and switchgrass. *Biomass and Bioenergy*, 27(4):339–352, 2004.

[70] Mei-Kuei Lee, Wen-Tien Tsai, Yi-Lin Tsai, and Sheau-Horng Lin. Pyrolysis of napier grass in an induction-heating reactor. *Journal of Analytical and Applied Pyrolysis*, 88(2):110–116, 2010.

[71] David A Laird, Robert C Brown, James E Amonette, and Johannes Lehmann. Review of the pyrolysis platform for coproducing bio-oil and biochar. *Biofuels, Bioproducts and Biorefining*, 3(5):547–562, 2009.

[72] FA Agblevor and S Besler. Inorganic compounds in biomass feedstocks. 1. effect on the quality of fast pyrolysis oils. *Energy & Fuels*, 10(2):293–298, 1996.

[73] FA Agblevor, S Besler, and AE Wiselogel. Fast pyrolysis of stored biomass feedstocks. *Energy & Fuels*, 9(4):635–640, 1995.

[74] Tristan R Brown, Rajeeva Thilakaratne, Robert C Brown, and Guiping Hu. Regional differences in the economic feasibility of advanced biorefineries: Fast pyrolysis and hydroprocessing. *Energy policy*, 57:234–243, 2013.

Appendix A

Pyrolysis Reactor Design and Troubleshooting

A.1 Design, Repair, and Upgrades

A.1.1 General

The fluid bed reactor, while functioning, does require some amount of maintenance to keep it running. Most joints under insulation are Swagelok compression fittings that will never have issue unless dismantled. There are some joints, easy to locate by the larger insulation wrapping, that use a 4 bolt flange. These fittings will rarely need new gaskets. At the time of writing, graphite sheeting was custom cut by hand to use as gasket material. These gaskets rarely see failure unless the reactor is physically moved. At the start of the project, the reactor was connected to the frame at 2 points, which allowed some degree of rotation or flex. In an attempt to improve rigidity, more contact points were created.

A third style of connection, sanitary fittings, is used to connect collection canisters and the condensing apparatus. These fittings operate at a temperature that is low enough to

allow the use of rubber gaskets. One exception is the connection from the gas filter to the condenser. This will see much higher temperature, and a Teflon PTFE gasket is used, though it will deform under heat. Much of the 1" diameter tubing is heated by rope heaters from OMEGA Engineering. An important distinction to note for any piping that needs to fit the reactor, for modification or replacement; the pipes used are 'TUBING' and not 'PIPE', and because of technical differences the connectors will not match. These are flexible heating elements in a fiberglass sheathing that will burn out and need to be replaced, as their life expectancy is not long (6 months - 2 years, depending on operations). Any heating element to be replaced will need to be re-wrapped in insulations material (currently mineral fiberglass). Common HVAC aluminum tape, from the local hardware store, was used to hold the insulation in place.

A.1.2 Electrical

At the time of writing, the unit draws more current than is available on the circuits. Extensions cords are used to route power to additional circuits. Depending on operations, circuits will still trip. This could be due to the age of the wiring on the unit, the age of the extension cords, or the age of the wires in the building. It is of highest importance that the mass flow controller (MFC) be on a separate, dedicated circuit that has no risk of tripping. The current MFC will not close the valve upon power loss. Due to this design parameter, losing power mid run will cause a surge of carrier gas flow and a significant portion of bed mass will be ejected into the cyclones. If funding becomes available, it is highly recommended to replace the wiring on the reactor systems and purchase new extension cords. Additionally, it is further recommended to install a fuse block as an extra level of protection for operators.

A.1.3 Hopper

Currently the system is set up so that a screw auger translates mass through a pipe to a drop hole. The system is gravity fed to the reactor from this point. At the time of writing, a spare motor has been located, and a secondary screw auger can be added for minimal cost. This dual-auger feeding system is mentioned for various reactors in literature, many of which are fast pyrolysis biomass reactors, and its implementation would allow for a much tighter control of mass flow into the bed. It would also control mass entry post run during the vapor sweep, and provide an extra level of protection against pressure related issues.

A.1.4 Pressure, Problems, Effects, and Solutions

For successful runs on the reactor, the delicate balance of pressure within the system must be maintained. The carrier gas is regulated to 40 psi before entering the MFC, where it is metered to some volume/minute. Gas then enters the preheating zone and makes it way to the distributor plate, which will cause a significant pressure drop. The reactor is operated at atmospheric pressure, and values obtained from pressure gages read less than 1 psi. While it may seem worthwhile to check for multiple pressure points throughout the vapor line, it is worth noting that particulate matter will plug gage tubing, and the reading will always be zero. However, it is the author's opinion that an effort be made to maintain one gage, so as to tell when there are problems with flow in the system. Pressure buildup in the reactor could be as benign as a reactor 'hiccup', where the flow will correct itself within a minute, or it could be the first indicator of a serious problem, such as the feed line melting down. Low pressure in the feed hopper will result from a poorly sealed hopper gasket, and will cause feedstock and bed material to back feed into the feeding tube. If the plastic section of the feeding tube melts, the bed material will erupt from the system, effectively bead blasting anything in its path. This same outcome can happen due to pressure buildup at the hot

gas filter. A small rise in back pressure, typically 1-3 psi, will break the seal on the hopper gasket and create flow problems. If all the hopper bolts are secured, the o-rings on the auger line are properly seated, and yet there is still a gas leak from the hopper, then the gas filter has reached its maximum load. The system will have to be cooled, and the filter will have to be properly cleaned. Regular cleaning of the filter will reliably prevent this problem on any short to mid duration run (1-6 hours or more). The maximum limit of the filter cake formation for back pressure is unknown and will vary on operating parameters and feedstock. When trying to balance pressure between the bed and hopper, recall that pressure will move from high zones to low zones; this principal should also be kept in mind for any changes in piping. It is worth noting that a fluid bed can be operated as a pressurized system, though this one is not designed for this purpose and modifications would be required.

A.1.5 Hot Gas Filter

The hot gas filter is worth any amount of maintenance it requires for the ash reduction abilities it provides to the liquid product. Over time, fly ash will accumulate on the filter screen, forming a filter cake. This cake may improve filter performance somewhat, but it will also increase the filter's pressure drop. Beyond a certain threshold, which is unknown and varies by operating parameters, the pressure build up will cause a leak elsewhere in the system. To counter this effect, regular maintenance of the filter must be performed. Removing the filter from the housing and back flowing air at 80-100 psi will remove most material. For more sterile cleansing, the filter can be reinstalled to the housing, and Zone 5 can be heated to 500°C. Install the airline to the reactor, sealing all other outlets except for the gas filter outlet, and turn the air on to 10 psi. Over the course of an hour, slowly increase the air flow to 60 psi and allow the system to burn the filter clean. Note that for a general system cleaning, the filter can be removed, all zones heated, and a much more aggressive burn method can be used. An alternative to the standard flow rate, the filter burn can be

done with backwards air flow, allowing the second solid cyclone to act as exhaust. Lastly, it may be necessary to clean with solvent. For this project in particular, where large amounts of red mud caked into the catalyst, distilled white vinegar was used to dissolve the iron based mud off.

A.1.6 Condensing

The glass condensed used prior to this project cracked after years of use and thermal stress. Under a lack of available funding, a spare stainless steel housing was built, and with the help of the engineering machine shop, connections were created to install this as part of the system. Copper tubing was purchased and was bent by hand to form three coils, maximizing available surface area in the housing. Tap water is passed through the condenser assembly and exits outside. Assuming that there is no reaction of pyrolysis vapors with copper, it is strongly suggested that funding be directed to other condensing upgrades, rather than purchasing a new glass condenser. In particular, a circulating coolant bath that is capable of reaching and maintaining subzero temperatures would improve the yield more so than a new glass condenser of similar design. Even more, an electrostatic precipitator (ESP) would provide a drastic change in yield values, with the potential to double yield mass.

A.1.7 Thoughts on Bed, Heat Transfer, and Bed Material

Two different bed materials were used during the course of this project. In an effort to maintain control, a parameter had to be defined to ensure these materials were equivalent. While mass is the preferred unit of reporting, the reactor can be thought of as operating in volumetric terms. Mass is fed into the system as a volumetric flow rate, though typically reported as mass flow rate. Carrier gas is fed as a volumetric flow rate, and exiting vapors are a volume, as well as a volume of liquid condensed. Thinking of the system in volumetric

terms, particularly with carrier gas and fluid dynamics, it was decided to designate a fixed bed height aspect ratio of 2:1, height to diameter.

Using the clear tube model, sand was fluxed until a satisfactory level of bubbling fluidization was achieved. This was repeated with red mud, aiming for a comparable level of bubbling activity. While sand can be classified as a Geldart B material, ground red mud follows Geldart A expectations, creating further problems with generating equivalent trials. Because it is a Geldart A, and because of its lower density, red mud had to be used with a larger particle size. Equivalent sizes were tested with sand and red mud. While the sand particles worked well, red mud in the 250 µm and lower range were so light that the divide between bed and freeboard was lost, and the result was a dust cloud of red mud throughout the length of the riser column. While this effect may have been desirable for catalysis, it was deemed unacceptable for the level of heat transfer required. For these reasons, a larger particle size was used for red mud. It may prove possible to use the same particle size and gas flow rate to achieve reasonably similar levels of fluidization, but time, in the form of testing and material preparations, prohibited this from being done.

The reactor was operated at a relatively slow speed, with the gearbox usually set to 1 or less. If higher feed rates are required it may be necessary to use a higher volume of bed material to act as a heat sink for the incoming mass. This will require adjustment of gas flow rates to maintain fluidization. It is worth noting that higher gas flow rates will decrease residence time, particularly of vapors, and will reduce secondary reactions. An alternative solution is to increase the heating ability of Zone 2 (the sand bed) which is currently heated with rope heaters. Other heating elements, such as the metal band heaters on Zone 5, may provide a higher heating rate to offset the higher influx of feedstock. Smaller particle sizes for sand are desirable to maximize the surface area/volume ratio of the sand. This is a balancing issue with bed attrition.

It was required to use the catalyst as an in-situ heat transfer material for this project.

Attrition rates are a function of the material itself and the gas flow rate. This allows a larger sample size to be sourced across multiple feedstocks allowing for a one-way ANOVA with two treatment options - sand and catalyst. ANOVA shown in Table A.1 shows statistical significance of the bed material as it relates to mass losses. Outliers were removed for runs of known distortion (spills, gas surge, etc) for ANOVA and produced mean mass losses of 14.23 g (13.10) for sand and 33.39 g (8.29) for red mud. In an effort to maintain integrity of

Table A.1: ANOVA - Bed Attrition

Source	df	SS	MS	F	Pr >F
Tt	1	0.0629	0.0629	33.8415	<.0001
Error	16	0.0297	0.0019	-	-
Total	17	0.0926	-	-	-

these numbers, standard time frames for warm-up, run time, and cool down were established so that all runs saw an equal loading rate of bed material and an equal run time for carrier gas. In addition to attrition rates, the high volatility of bio-char produced in catalyst runs suggest that red mud is not a suitable bed material. The data indicates that breakdown and loss of bed material is high enough that run times would be significantly limited when red mud was used without in-run replacement. In addition to this, the high volatility of the bio-char suggests that pyrolysis is not being achieved to the same level as with sand. These two factors lead to a recommendation that red mud as presented in this paper not be used as bed material without prior modification. These modifications should aim to effect density and durability. Heat transfer is a function of electrons, not density, and the question remains as to whether red mud failed to pyrolyze as well as sand due to its physical composition, or if density and fluidization of the larger particles, relative to sand, can explain these deviances. With the availability of an external furnace, it may be advisable to investigate red mud ex-situ through either a secondary fluid bed, or a packed bed downstream from the hot gas filter.

Appendix B

Statistical Analysis

Table B.1: ANOVA - Ash reduction via water washing

Source	df	SS	MS	F	Pr >F
Treatment	1	8.4125	8.4125	51.2426**	<.0001
Error	11	1.8059	0.1642	-	-
Total	12	10.2184	-	-	-

Table B.2: ANOVA - Liquid yields of Control and WaterWash groups

Source	df	SS	MS	F	Pr >F
Catalyst	1	0.0042	0.0042	24.2602**	0.0079
Group	1	0.0013	0.0013	7.8805*	0.0485
Interaction	1	0.0003	0.0003	1.7030	0.2619
Error	4	0.0007	0.0002	-	-
Total	7	0.0065	-	-	-

Table B.3: ANOVA - Levoglucosan production, water wash vs. control

Source	df	SS	MS	F	Pr >F
Catalyst	1	43958.2276	43958.2276	143.1866**	<0.0001
Group	1	45306.0271	45306.0271	147.5769**	<0.0001
Interaction	1	13539.4809	13539.4809	44.1026**	<0.0001
Error	12	3683.9942	306.9995	-	-
Total	15	106487.7298	-	-	-

Table B.4: ANOVA - Formate production, water wash vs. control

Source	df	SS	MS	F	Pr >F
Catalyst	1	5416.9526	5416.9526	6.3791*	0.0266
Group	1	9489.9160	9489.9160	11.1756**	0.0059
Interaction	1	868.0625	868.0625	1.0223	0.3319
Error	12	10190.0002	849.1667	-	-
Total	15	25964.9313	-	-	-

Table B.5: ANOVA - Acetate production, water wash vs. control

Source	df	SS	MS	F	Pr >F
Catalyst	1	4555.2916	4555.2916	16.4473**	0.0016
Group	1	10234.7315	10234.7315	36.9535**	<0.0001
Interaction	1	35.5144	35.5144	0.1282	0.7265
Error	12	3323.5535	276.9628	-	-
Total	15	18149.0910	-	-	-

Table B.6: ANOVA - Hydroxyacetone production, water wash vs. control

Source	df	SS	MS	F	Pr >F
Catalyst	1	956.5396	956.5396	10.7998**	0.0065
Group	1	1762.9061	1762.9061	19.9040**	0.0008
Interaction	1	44.2016	44.2016	0.4991	0.4934
Error	12	1062.8430	88.5703	-	-
Total	15	3826.4903	-	-	-

Table B.7: ANOVA - Liquid yields of WaterWash, T250, and T275

Source	df	SS	MS	F	Pr >F
Catalyst	1	0.0128	0.0128	29.8425**	0.0016
Group	2	0.0153	0.0077	17.9061**	0.0030
Interaction	2	0.0021	0.0011	2.5070	0.1617
Error	6	0.0026	0.0004	-	-
Total	11	0.0328	-	-	-

Table B.8: ANOVA - Levoglucosan production, WW vs. T250 vs. T275

Source	df	SS	MS	F	Pr >F
Catalyst	1	101931.8887	101931.8887	130.0108**	<0.0001
Group	2	8012.2570	4006.1285	5.1097*	0.0175
Interaction	2	3743.8712	1871.9356	2.3876	0.1203
Error	18	14112.4686	784.0260	-	-
Total	23	127800.4855	-	-	-

Table B.9: ANOVA - Formate production, WW vs. T250 vs. T275

Source	df	SS	MS	F	Pr >F
Catalyst	1	295.9310	295.9310	0.2757	0.6059
Group	2	22267.7743	11133.8872	10.3720**	0.0010
Interaction	2	70097.1063	35048.5531	32.6503**	<0.0001
Error	18	19322.1284	1073.4516	-	-
Total	23	111982.9400	-	-	-

Table B.10: ANOVA - Acetate production, WW vs. T250 vs. T275

Source	df	SS	MS	F	Pr >F
Catalyst	1	208.3936	208.3936	0.6232	0.4401
Group	2	37241.1778	18620.5889	55.6856**	<0.0001
Interaction	2	138969.8488	69484.9244	207.7973**	<0.0001
Error	18	6018.9855	334.3881	-	-
Total	23	182438.4057	-	-	-

Table B.11: ANOVA - Hydroxyacetone production, WW vs. T250 vs. T275

Source	df	SS	MS	F	Pr >F
Catalyst	1	78.4799	78.4799	0.8443	0.3703
Group	2	8718.0471	4359.0235	46.8939**	<0.0001
Interaction	2	32454.6878	16227.3439	174.5720**	<0.0001
Error	18	1673.1900	92.9550	-	-
Total	23	42924.4047	-	-	-

Appendix C

GC-MS Raw Data

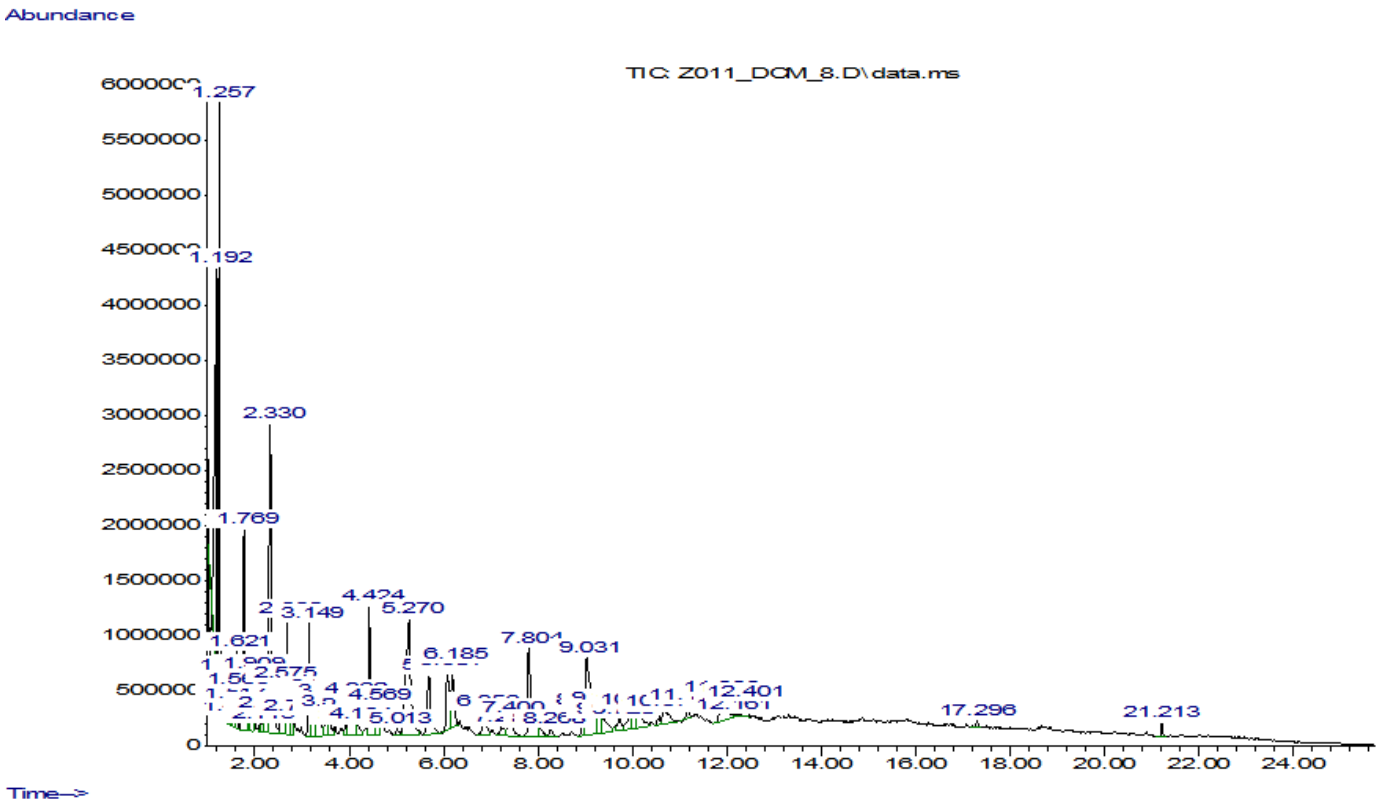

Figure C.1: Chromatogram of DCM fraction

Table C.1: Retention Times by Compound, DCM Fraction

RT (min)	Hit Name
1.191	Acetic acid
1.258	2-Propanone, 1-hydroxy-
1.319	2,3-Pentanedione
1.412	Acetic acid, methoxy-, ethyl ester
1.463	Propenoic acid, 2-trifluoroacetylamino-
1.519	Propanoic acid
1.56	Propanoic acid
1.622	Butanoic acid, methyl ester
1.771	(S)-(+)-3-Hydroxytetrahydrofuran
1.863	3-Furanol, tetrahydro-
1.909	2-Hexene
2.114	Furfural
2.171	1-Butanol, 2,3-dimethyl-
2.248	2-Propenoic acid, 2-methyl-
2.33	Furfural
2.576	5,9-Dodecadien-2-one, 6,10-dimethyl-, (E,E))-
2.689	1,2-Ethanediol, diacetate
2.791	1,4-Hexadiene, 4-methyl-
3.15	2-Cyclopenten-1-one, 2-methyl-
3.222	Ethanone, 1-(2-furanyl)-
3.335	Butyrolactone
3.519	2-Cyclopenten-1-one, 2-hydroxy-
3.576	2,4-Hexadiene, 2,3-dimethyl-
3.93	1-Methoxy-1-buten-3-yne
4.063	2-Cyclopenten-1-one, 3-methyl-
4.166	2-Cyclopenten-1-one, 3-methyl-
4.422	Phenol
4.571	Phenol
5.012	1-Methoxy-1,3-cyclohexadiene
5.268	2-Cyclopenten-1-one, 2-hydroxy-3-methyl-
5.694	Phenol, 2-methyl-
6.079	Phenol, 4-methyl-
6.186	Phenol, 2-methoxy-
6.858	2-Cyclopenten-1-one, 3-ethyl-2-hydroxy-
7.222	Phenol, 2-ethyl-
7.402	Phenol, 2,4-dimethyl-
7.802	Phenol, 4-ethyl-
8.043	Phenol, 3-ethyl-
8.269	Phenol, 2-methoxy-4-methyl-
8.956	1,2-Benzenediol
9.033	Benzofuran, 2,3-dihydro-
9.284	Phenol, 2-ethyl-6-methyl-
9.397	Phenol, 2-ethoxy-
9.73	Phenol, 2-ethoxy-
9.951	5-Isopropyl-3,3-dimethyl-2-methylene-2,3-dihydrofuran
10.038	1,2-Benzenediol, 4-methyl-
10.11	1,2-Benzenediol, 3-methyl-
10.546	Ethanone, 1-(3-methoxyphenyl)-
10.669	1,2-Benzenediol, 4-methyl-
11.167	Phenol, 2,6-dimethoxy-
11.89	Benzene, 2-fluoro-1,3,5-trimethyl-
12.162	Benzene, 2-fluoro-1,3,5-trimethyl-
12.403	Cyclopropanecarboxylic acid, 2,2-dimethyl-3-(2-methyl-1-propenyl)-
17.295	1H-Cycloprop[e]azulene, decahydro-1,1,7-trimethyl-4-methylene-, [1aR-(1a.alpha.,4a.beta.,7.alpha.,7a.beta.,7b.alpha.)]-
21.214	Oxirane, 2,2'-[(1-methylethylidene)bis(4,1-phenyleneoxymethylene)]bis-

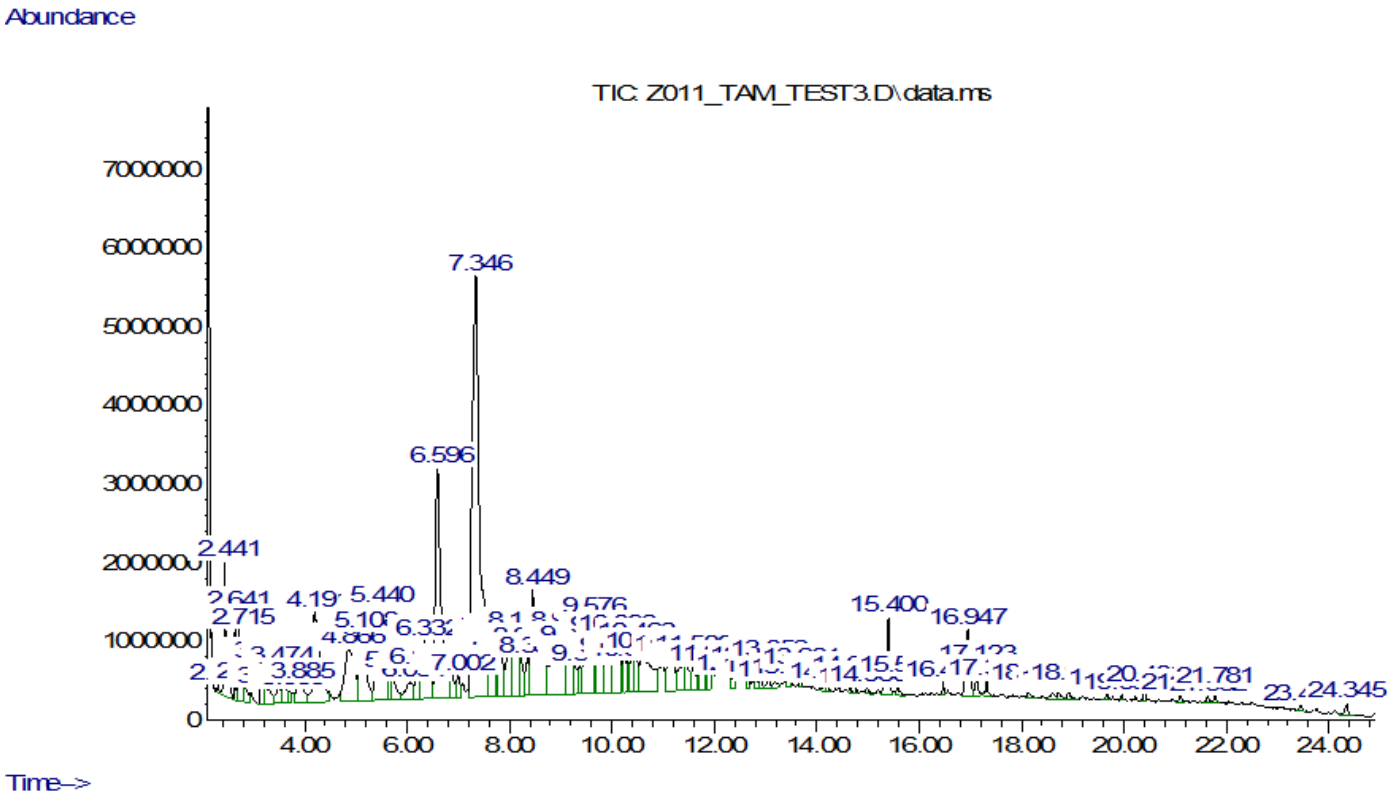

Figure C.2: Chromatogram of TAM fraction

Table C.2: Retention Times by Compound, TAM Fraction

RT (min)	Hit Name	RT (min)	Hit Name
2.306	Propanoic acid, 3-hydroxy-	10.302	1,5-Dihydroxy-1,2,3,4-tetrahydronaphthalene
2.439	Furfural	10.384	Pyrrolidine, 1-(1-cyclopenten-1-yl)-
2.64	Ethylbenzene	10.461	2,3-Diethylpyrazine
2.716	Benzene, 1,3-dimethyl-	10.605	2,3-Dimethylanisole
2.824	1,6;2,3-Dianhydro-4-O-acetyl-.beta.-d-gulopyranose	11.164	Indanone, 2-hydroxyimino
3.163	2-Cyclopenten-1-one, 2-methyl-	11.389	N-(1-Cyclohexen-1-yl)piperidine
3.219	2,4-Hexadiene, 2,5-dimethyl-	11.446	5-Methoxy-4-methyl-2,1,3-benzothiadiazole
3.475	N-Formylmorpholine	11.589	1-Hexadecene
3.609	Pyrrolin-2-one-5-methanol, N-methyl-	11.774	Imidazole, 2-methyl-4-trifluoromethyl-
3.691	Benzamide, 2-amino-N-[2-(1-piperidyl)ethyl]-	11.82	2-Benzothiazolamine
3.886	2-Furancarboxaldehyde, 5-methyl-	11.851	2-Benzothiazolamine
4.194	Phenol	12.379	1-Benzyl-1H-1,2,4-triazole
4.865	1,2-Cyclopentanedione, 3-methyl-	12.661	Cyclododecane, ethyl-
5.106	Phenol, 2-methyl-	12.83	Quinoline, 6-methoxy-, 1-oxide
5.44	Phenol, 3-methyl-	12.907	1H-Benzimidazole, 2-phenyl-
5.655	Phenol, 2-methyl-	13.056	7-Tetradecene, (Z)-
5.717	Phenol, 2,5-dimethyl-	13.184	Benzene, 1-bromo-4-methyl-
6.055	2-Cyclopenten-1-one, 3-ethyl-2-hydroxy-	13.456	s-Triazolo[4,3-a]pyridine, 3-ethyl-5-methyl-
6.194	Phenol, 3,5-dimethyl-	13.682	Z-8-Hexadecene
6.332	Phenol, 2,4-dimethyl-	14.138	Tetrahydroionone
6.594	Phenol, 4-ethyl-	14.22	3,4-Dichloroisocoumarin
6.871	Phenol, 2-methoxy-4-methyl-	14.651	1-Nonadecene
7.004	Benzene, 1-methoxy-4-methyl-	14.779	2-(4a,8-Dimethyl-6-oxo-1,2,3,4,4a,5,6,8a-octahydro-naphthalen-2-yl)-propionaldehyde
7.348	Benzofuran, 2,3-dihydro-	14.979	Methyl 10-methyl-undecanoate
7.604	1,2-Benzenediol	15.4	n-Hexadecanoic acid
7.763	Phenol, 2-propyl-	15.585	Carbonic acid, octadecyl 2,2,2-trichloroethyl ester
7.814	1,4-Benzenedicarboxaldehyde, 2-methyl-	16.472	1-Nonadecene
8.02	O-Methoxy-.alpha.-methylbenzyl alcohol	16.949	6-Octadecenoic acid
8.127	1,2-Benzenediol, 4-methyl-	17.123	Octadecanoic acid
8.209	Benzofuran, 2,3-dihydro-2-methyl-	17.323	1-Eicosene
8.348	Benzocycloheptatriene	18.139	Z-5-Nonadecene
8.45	2-Methoxy-4-vinylphenol	18.611	Palladium, (.eta.-3-allyl)-isopropylcyclopentadienyl-
8.968	2-Propenoic acid, 3-(3-hydroxyphenyl)-	18.723	Eicosanoic acid
9.133	Benzofuran, 7-methyl-	18.923	1-Eicosene
9.276	2,3-Dimethylhydroquinone	19.672	1-Eicosene
9.374	Phenol, 2-(methylsulfinyl)-	19.954	Oxirane, hexadecyl-
9.574	1-(2,4-Dimethyl-furan-3-yl)-ethanone	20.401	1-Nonadecene
9.681	1-(2,4-Dimethyl-furan-3-yl)-ethanone	21.103	1-Octadecanethiol
9.722	2-Methoxy-6-methylphenol	21.631	6-Cholro-2-cyclohexyl-4[3H]quinazolinone
9.922	Benzene, 2-fluoro-1,3,5-trimethyl-	21.78	1-Docosene
10.092	Eugenol	23.457	(1R,2S,8As)-8-oxo-1-carboxymethyl-1,2,5,5-tetramethyl-trans-decalin
10.256	Pyrazine, 2-methoxy-3-(1-methylethyl)-	24.345	Stigmastan-3,5-diene

Appendix D

HPLC Raw Data

Representative raw HPLC files are presented below to display the full array of peaks and unknowns.

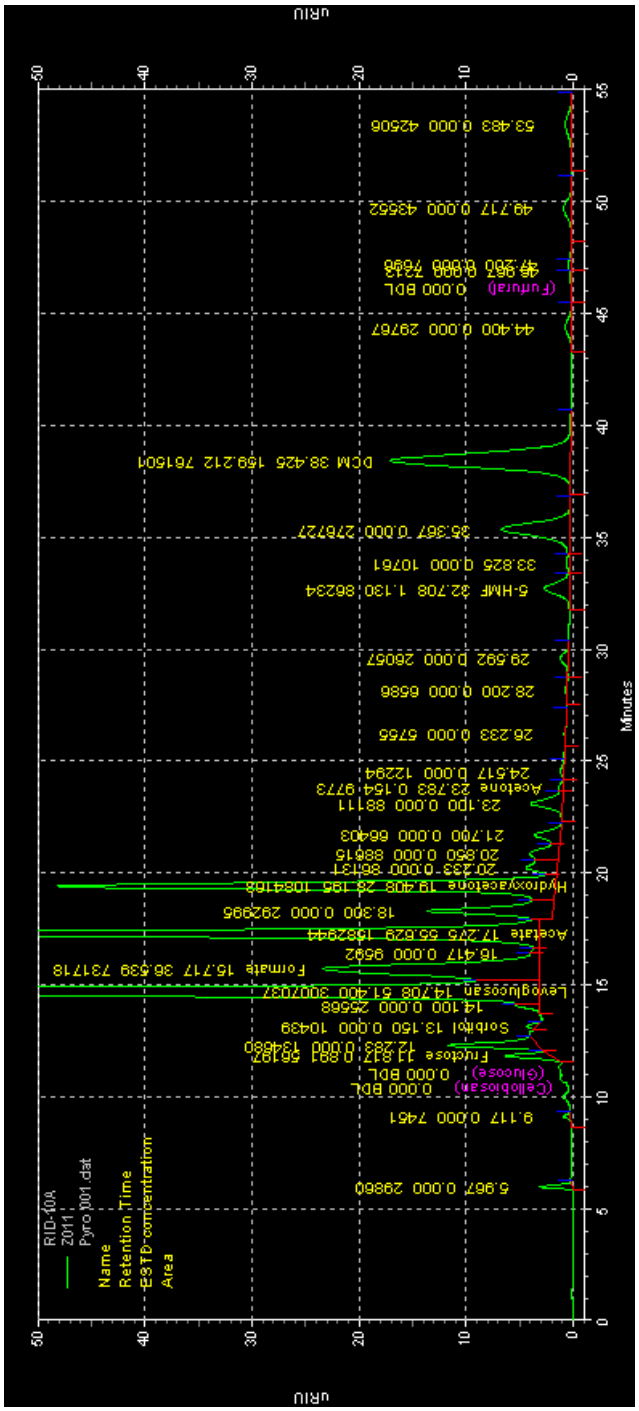

Figure D.1: Energy Cane Control, Rep 1

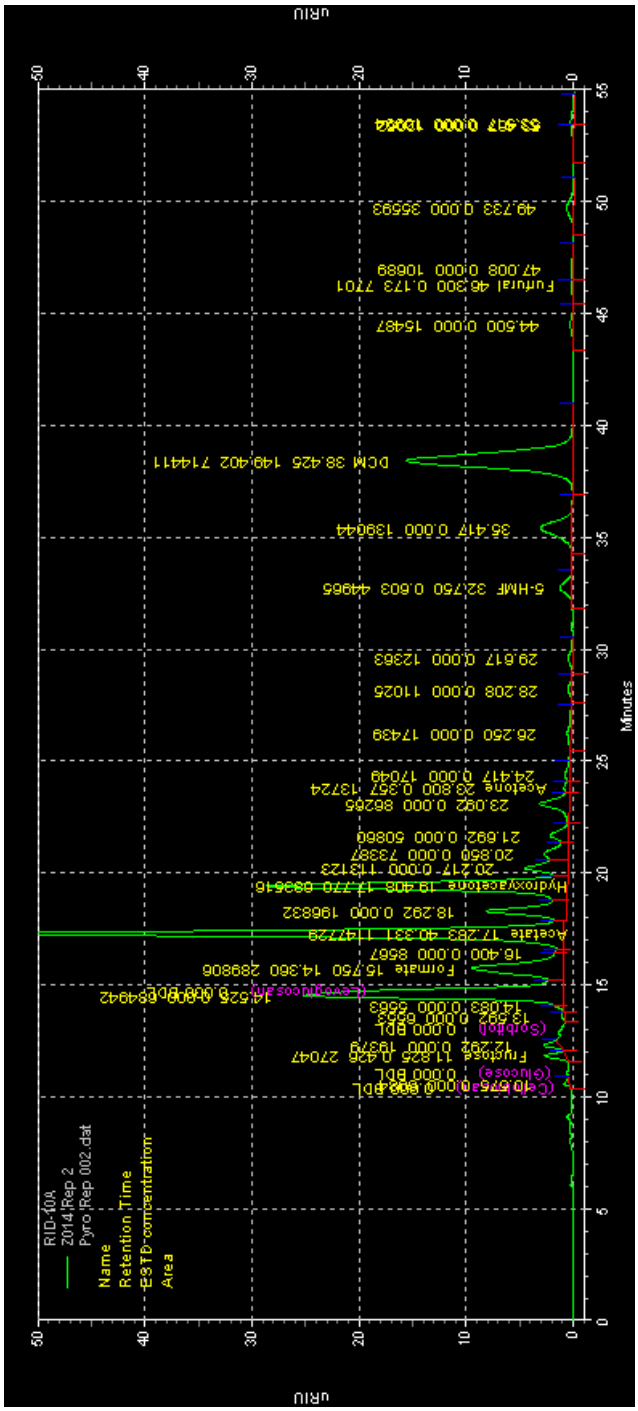

Figure D.2: Energy Cane Catalyst, Rep 2

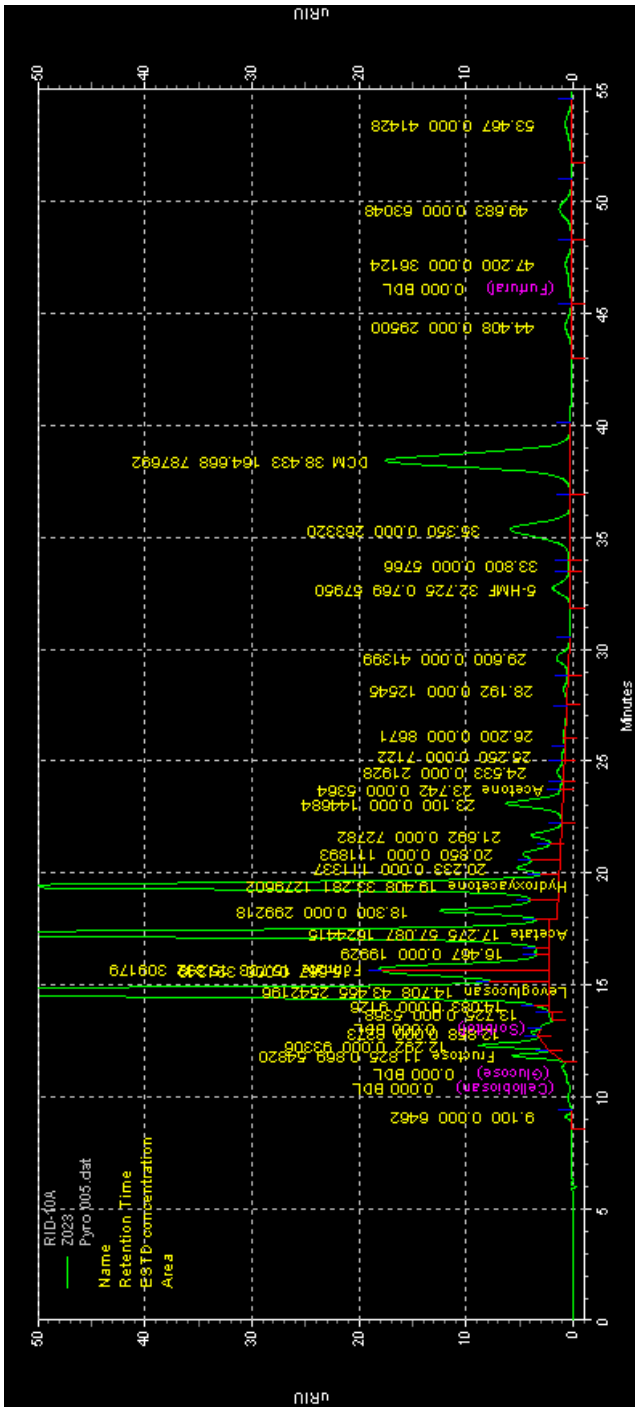

Figure D.3: Elephant Grass Control-2, Rep 1

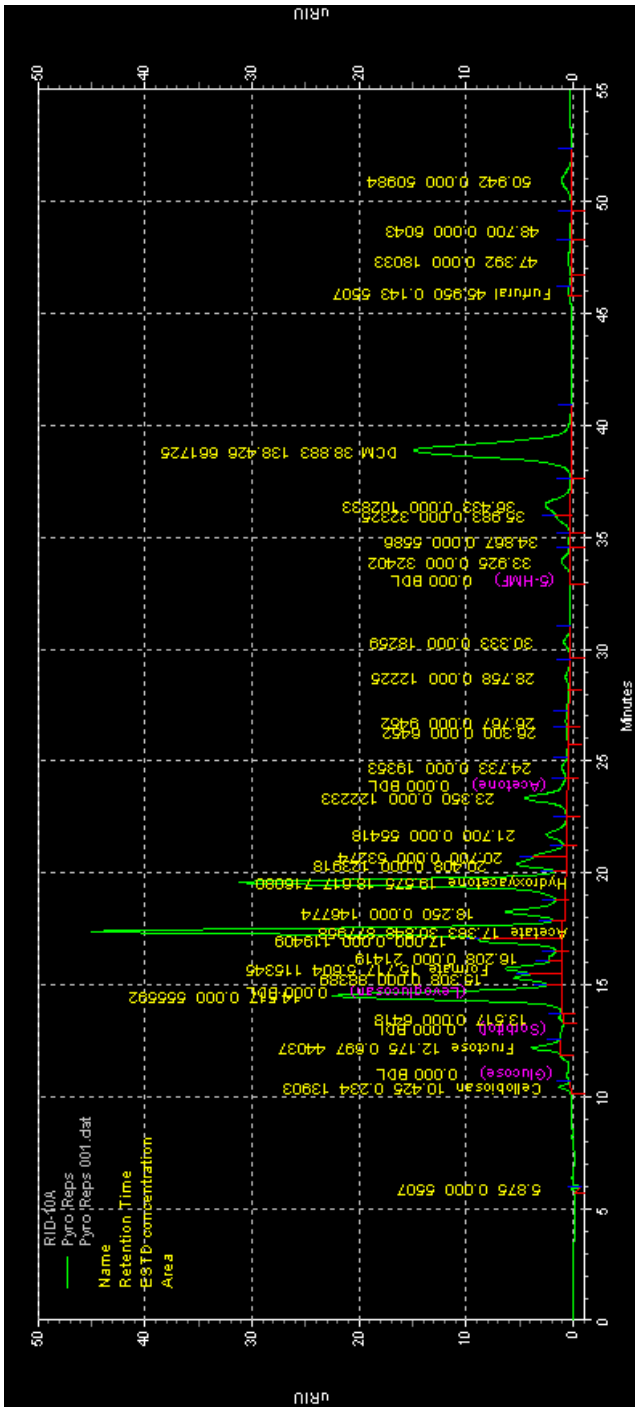

Figure D.4: Elephant Grass Catalyst-2, Rep 2

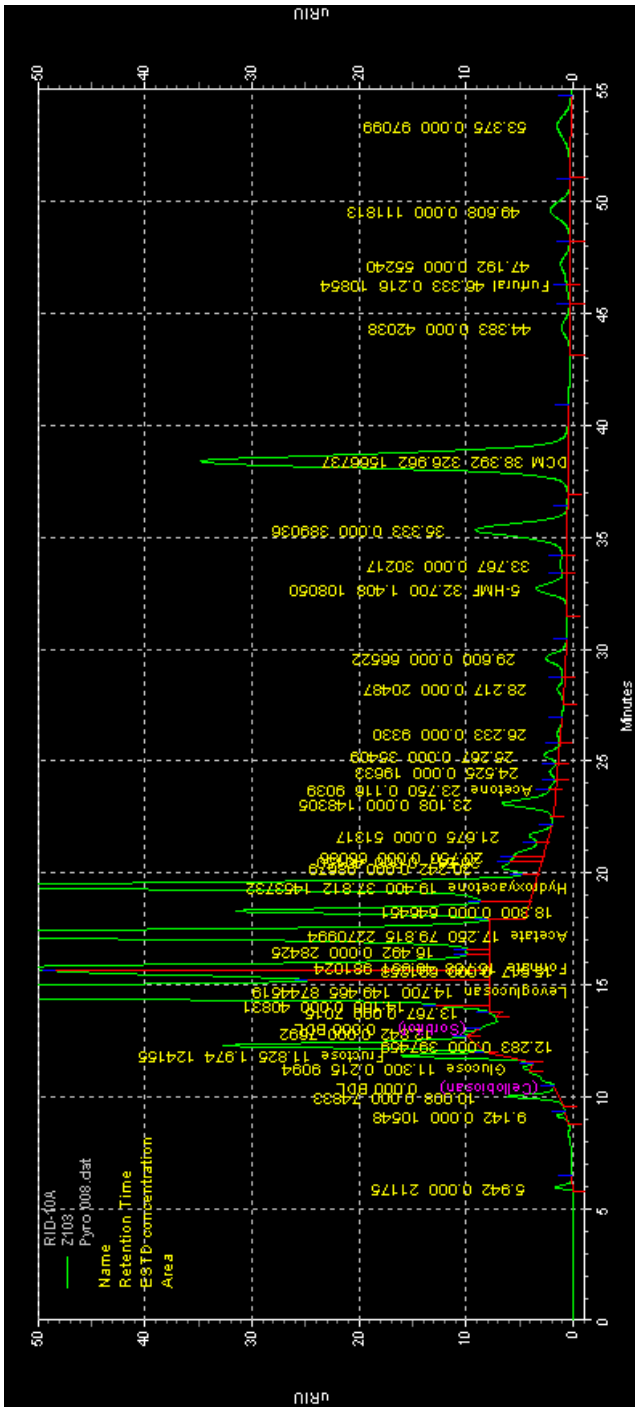

Figure D.5: Water Wash Control-1, Rep 1

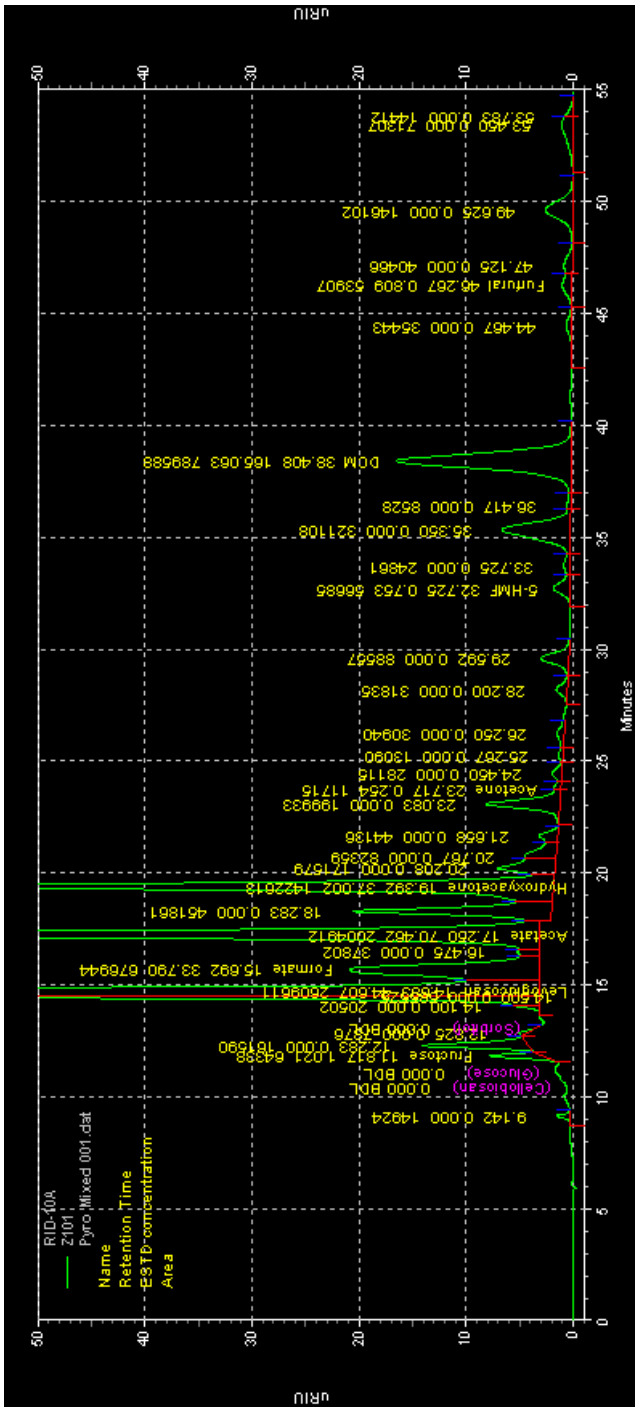

Figure D.6: Water Wash Catalyst-1, Rep 2

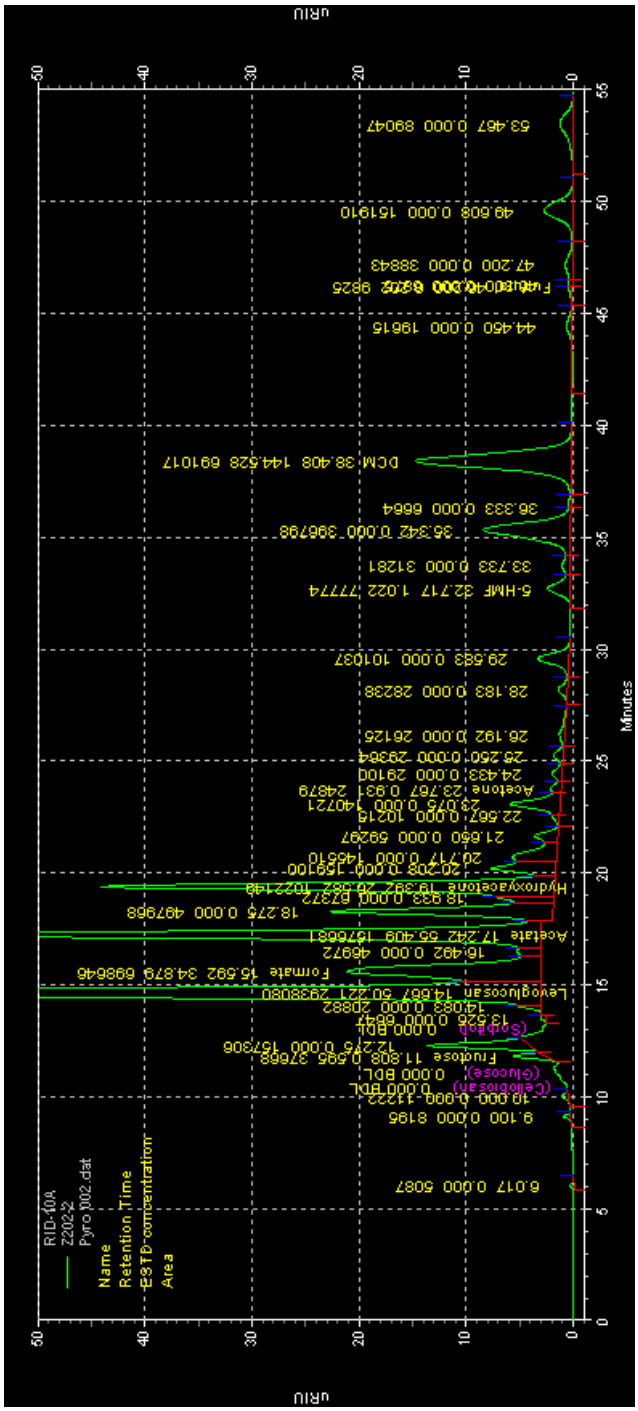

Figure D.7: T250 Catalyst-1, Rep 2

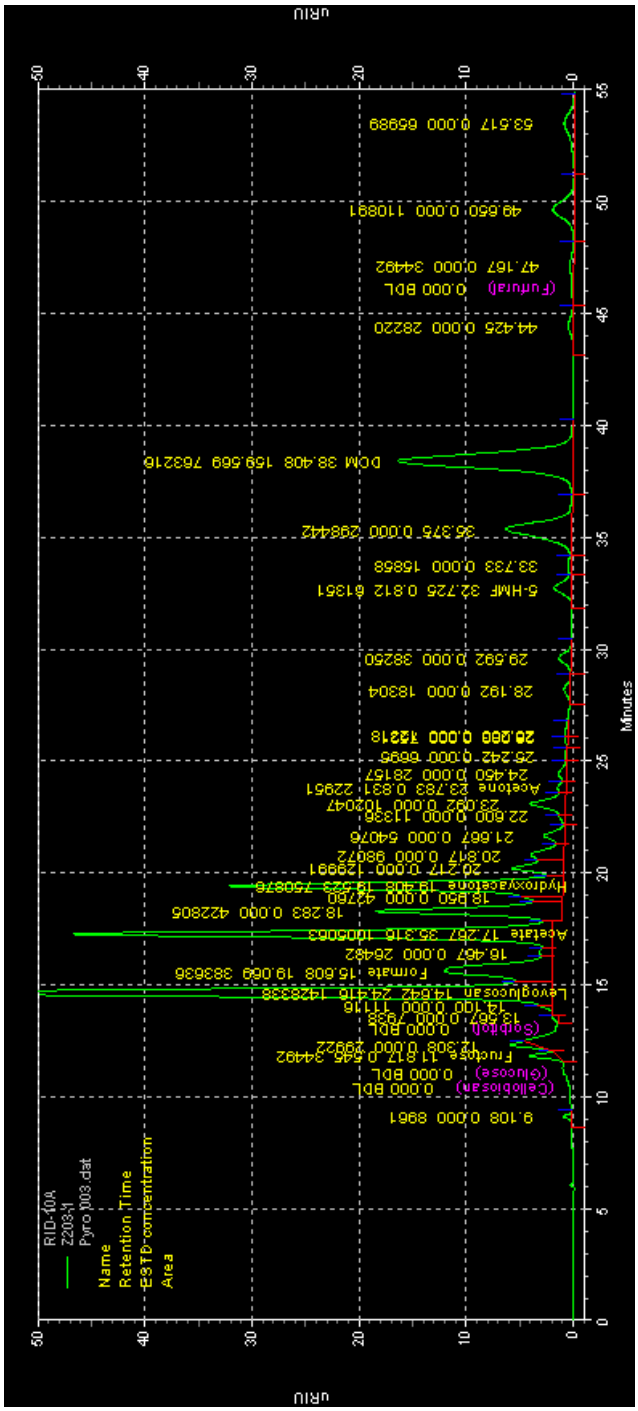

Figure D.8: T250 Catalyst-2, Rep 1

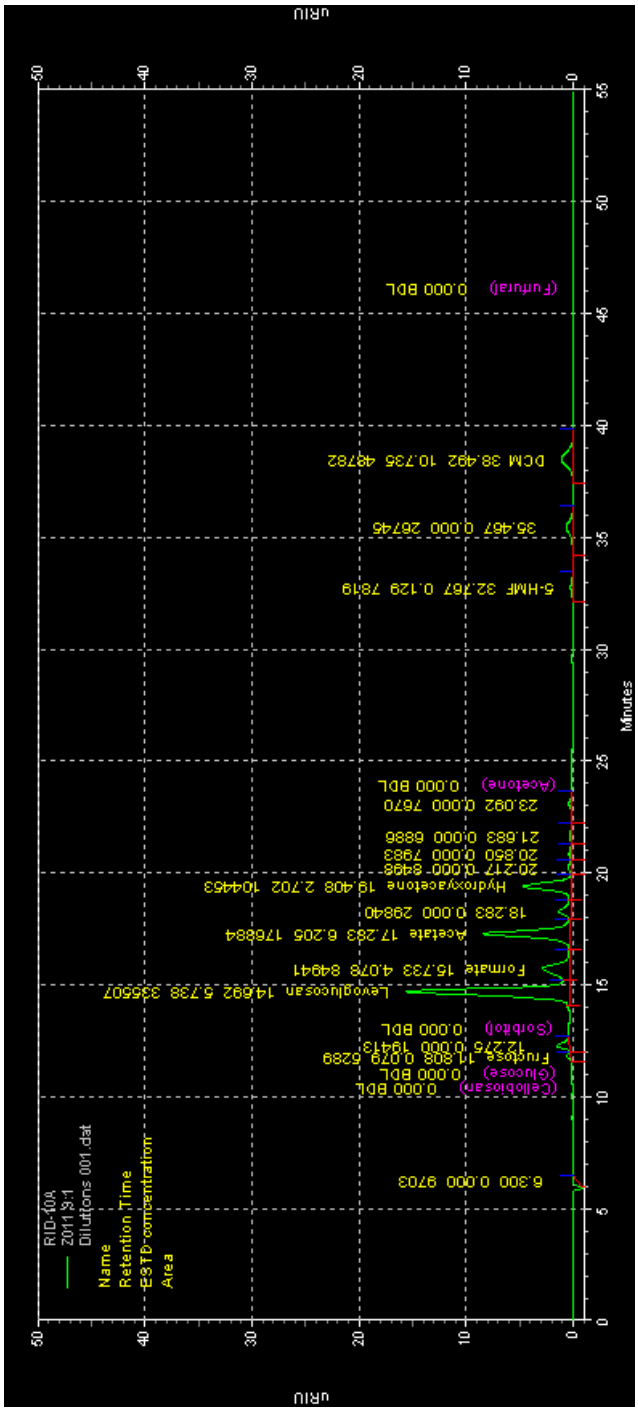

Figure D.9: Energy Cane Control, Diluted, Rep 1

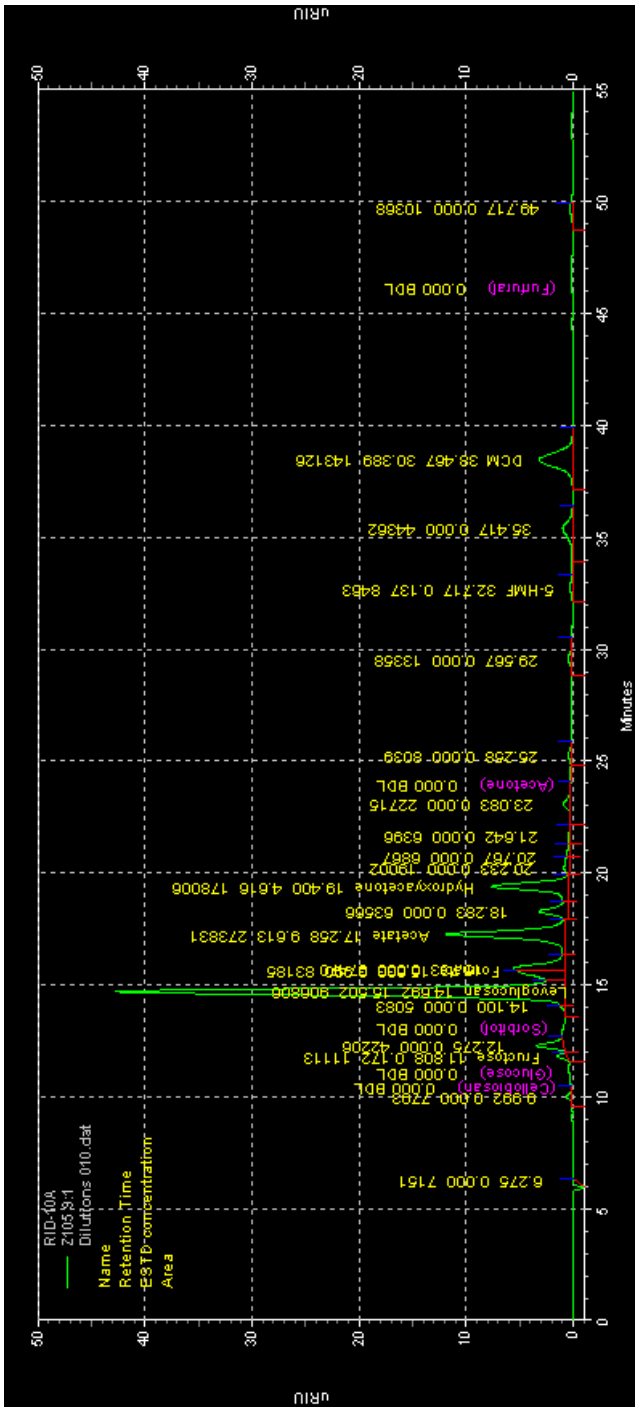

Figure D.10: Water Wash Control-2, Diluted, Rep 1

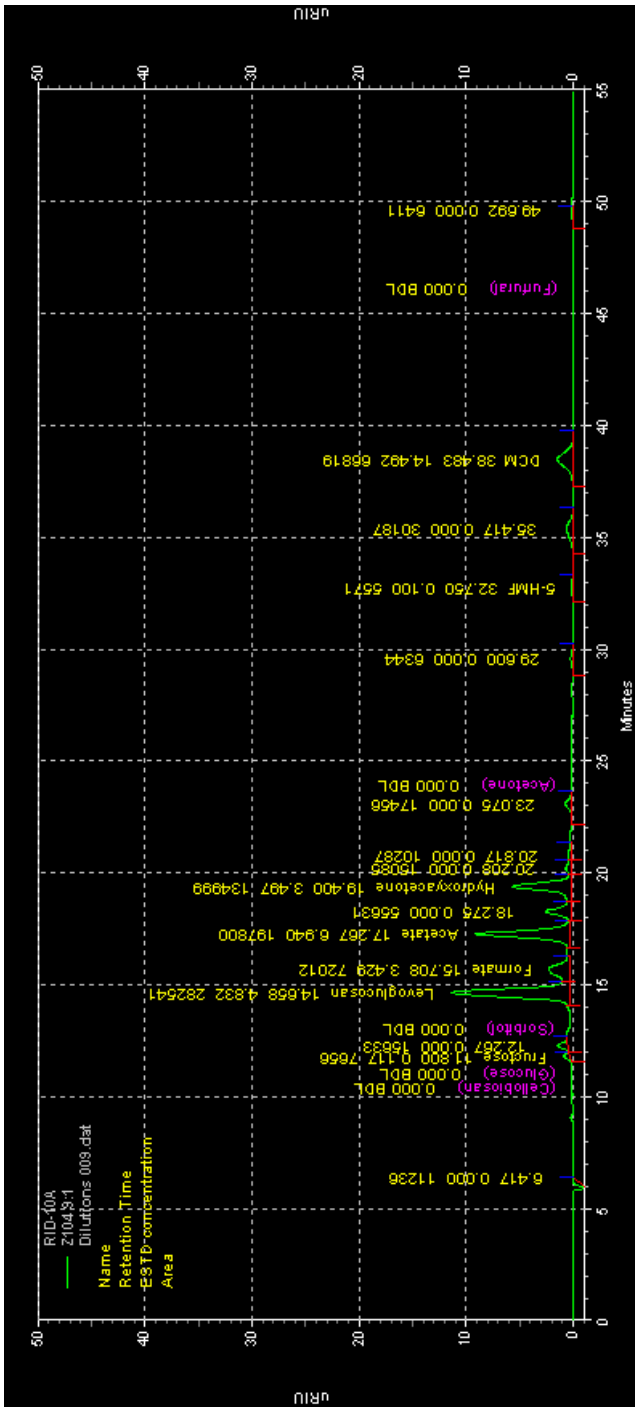

Figure D.11: Water Wash Catalyst-2, Diluted, Rep 1

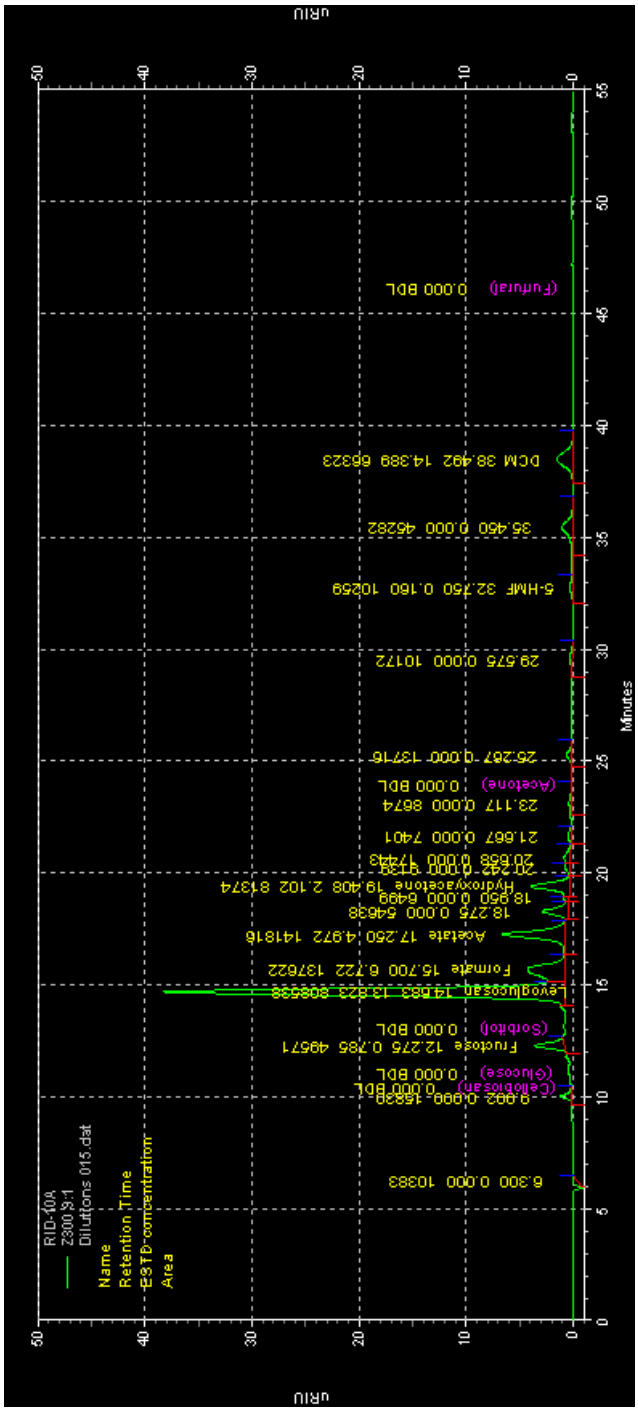

Figure D.12: T275 Control-1, Diluted, Rep 1

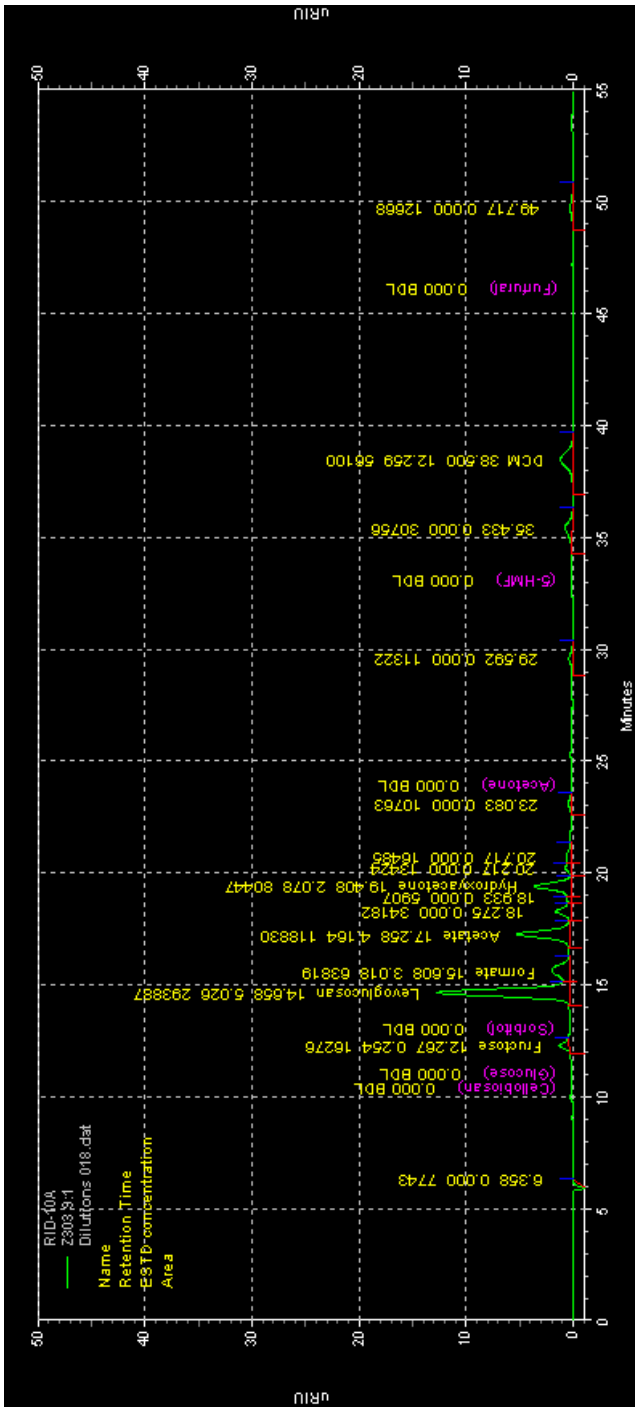

Figure D.13: T275 Catalyst-2, Diluted, Rep 1